2018

Physical modeling of lithium-ion aging for automotive applications

Anurag Kamal
Michigan Technological University, akamal@mtu.edu

PHYSICAL MODELING OF LITHIUM-ION AGING

FOR AUTOMOTIVE APPLICATIONS

By

Anurag Kamal

A THESIS

Submitted in partial fulfillment of the requirements for the degree of

MASTER OF SCIENCE

In Mechanical Engineering

MICHIGAN TECHNOLOGICAL UNIVERSITY

2018

This thesis has been approved in partial fulfillment of the requirements for the Degree of MASTER OF SCIENCE in Mechanical engineering.

Department of Mechanical Engineering-Engineering Mechanics.

Thesis Advisor:	*Lucia Gauchia*
Committee Member:	*Erik Herbert*
Committee Member:	*Mahdi Shahbakhti*
Department Chair:	*William Predebon*

"Dedicated to my Father, Surendra N. Sinha,

I hope my work makes him proud."

Table of Contents

List of figures

List of tables

Acknowledgements

It has been a great time with highs and lows at my graduate school. It delights me to acknowledge all the support I got in this wonderful journey.

Michigan Tech and the department of Mechanical engineering have surpassed my expectations from a graduate school. The collegiate organizations and the entrepreneurship club have groomed me towards my career goals, more than I anticipated.

I would like to express my sincere gratitude to my advisor, Dr. Lucia Gauchia. She has always been supportive of my initiatives to choose my own direction of research. She provided me with opportunities and resources to keep my work eclectic. Her enthusiasm in the field of energy storage has been my source of inspiration through my research years.

Tough got easy with the people at Tech, they are friendly and bright. I must take this opportunity to thank the friends I have made here, they would last me a lifetime.

I would like to thank the committee members, Dr. Erik Herbert and Dr. Mahdi Shahbakhti for taking time from their schedules to review my work and contributing to its refinement. Their feedback helped me model the future direction of my thesis.

I couldn't possibly express all of my gratitude to my family. My parents have been there through thick and thin, supporting my career choices. My time at the States wouldn't have been possible without my dear brother's endless support and career founding conversations.

Finally, I must thank the other important people who have gone unmentioned, for shaping my life the way they do. Also, to the ruined batteries, burnt boards, and the wasted processing power, I hope it was for the greater good.

Anurag Kamal

List of abbreviations

LIB – Lithium-ion batteries
SOC- State of Charge
EQM- Equivalent Circuit modeling
SPM- Single Particle Model
PDE- Partial Differential Equations
SEI- Solid electrolyte layer
BMS- Battery Management System
LFP- Lithium iron phosphate
EIS - Electrochemical impedance spectroscopy
NMC- Lithium Nickel Manganese Cobalt
DOD- Depth of Discharge
EVS- Impedance spectroscopy with voltage
NMR- Nuclear magnetic response spectroscopy
BMS- Battery Management System
OCV- Open Circuit Voltage
MOR- Model order reduction

Abstract

As the world makes a slow transition from conventional sources to renewable energy, the need for energy storage is climbing. The role of battery modeling becomes more critical, not only for predicting the state variables of existing battery systems, but also to aid the development of new battery systems by a deeper understanding of the chemical processes that make up a cell.

This thesis extends the full-scale electrochemical model for Lithium-ion battery based on the porous electrode theory to incorporate aging mechanisms of solid electrolyte interface formation, cyclic electrode degradation, and lithium plating during overcharge, automotive vibrations, mechanical stress and cell temperature, as reported in the existing literature. Further, the thesis presents the scope of the parameters used in the model to enable designers to extend the equations for new mechanisms and variability of other parameters.

An increased set of equations makes the complexity of the model even higher, and it would be very computationally complex to simulate this model. This makes this model unsuitable for inexpensive processors of mobile applications like an automotive battery management system, while increasing the uncertainty faced by PDE solvers. However, as the physical models get close to an actual lithium-ion battery behavior, they could accelerate its development, shortening the design life of batteries.

1 Introduction

Lithium ion batteries (LIB) are the current workhorse of the mobile energy storage industry. Since their ideation in 1970's, there has been continuous research going on to increase their capacity and the aging behavior. The current literatures address the domains of electrodes [1], electrolytes[2] and the separator [3], to make batteries more energy dense, safe, and long lasting. Even though the major internal phenomena happening through the battery are known, there are still mechanisms of degradation and side reactions, that are unquantified [4][5]. The battery is a closed boundary mass exchange system, and direct measurement or observance of majority of the intended and unintended phenomenon is not possible. Hence, there is a need of models which can closely represent the battery's real performance, so that LIB could be put to an optimized usage which is safe and long lasting [6] .

There have been many proposed methods to approach this challenge [7]–[10]. Majorly, there can be sorted into two types: statistical models [11] [12], and electrochemical model [13] [14]. The statistical models depend on the availability of plenty of testing data in a variety of conditions, which are not generally available, especially for new battery chemistries. The electrochemical modeling, however, depends on governing equations proposed by scientists over the last decades that predict the migration of charge and species inside a battery, and the degradation of these mechanisms over time. There is a plethora of phenomena that have been tamed with the governing equations [15] [7] [16] [17] [18], and this work is an approach to bring them together.

1.1 Scope of the thesis

The aim of this research is to document and tabulate interwoven work predicted for a lithium ion battery, and to mathematically couple them for implementation with the partial differential equation (PDE) based porous electrode theory [19]. This reference model could be helpful for battery researchers. As the physical model keep simulating a realistic LIB behavior, it could accelerate the development of LIB, as the design iterations of prototyping and testing could be eliminated.

The next chapter of the thesis discusses the development of a continuum scale model, and the reduction of the model into state space. A single particle model is also developed for drawing comparisons with the rest of the two models. Chapter 3 develops a novel model to integrate the existing methods of degradation to develop a full-scale model which incorporates multiple aging mechanisms with the porous electrode theory.

Chapter 4 presents a summary of the existing parameters required for the continuum scale model for different battery chemistries. The parameter estimation techniques are briefly discussed, and the parameters used for developing the final continuum scale model are mentioned. Chapter 5 documents the trials of development of the model, and enlists results generated with the model. The final chapter summarizes the findings of the work and suggests the future direction of this work.

1.2 Basics of a lithium-ion battery (LIB)

The class of batteries could be divided in two broad categories: primary and secondary batteries. The former are the energy storage devices intended for single usage such as zinc chloride, mercury batteries which find use in our watches, and remotes. The latter are the ones which could go through a charge and discharge cycles, like the automotive lead-acid battery, and Li-ion cells, etc.

This mechanism is generally referred as a rocking-chair mechanism, because of the cycling of electrons and ions from one electrode to the other through a series of reversible reactions (irreversible reactions are basically the cause of aging or the death of batteries). Figure 1-1 shows the basic schematic of a Lithium-ion battery. It consists of 3 basic parts, the negative and the positive electrode, and the separator. Electrolyte flushes the rest of the remaining gaps, and the space left between the electrodes as they are porous solids for increasing the surface area available for chemical processes. There are current collectors on both ends of the electrodes to facilitate the transfer of electrons to the external circuit. The separator is a special barrier that doesn't allow the flow of electrons inside the battery and lets the lithium ions pass unhindered.

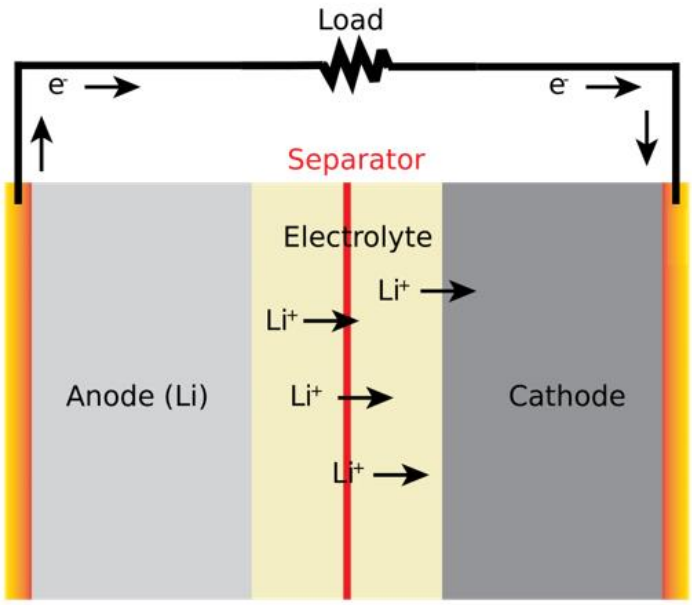

Figure 1-1 Li-ion battery schematic, the golden representations are current collectors

As the battery is put through an external load, the electrons flow from the negative to the positive current collector, creating an excess of electrons at one end. This makes positively charged Li-ions migrate from inside the cell to the positive electrode to keep the charge balance. While charging, this process is reversed when the external flow of electrons to the negative electrode makes the lithium ions to migrate back.

The negative electrode (or the anode during discharging process) could be made of carbon, silicon, and the cathodes have variety of choices with different chemistries like Lithium iron phosphate (LFP), Lithium manganese oxide (LMO), Lithium Cobalt oxide (LCO). The quality of a good electrode would be good cycling behavior (i.e. retaining the structural integrity with mechanical stress of intercalation cycling), low internal resistance, and high surface area to name a few [20], [21]. The electrolyte is generally a liquid made of a Lithium-salt with an organic solvent like dimethyl carbonate, and the properties required of them are to be stable at high temperatures and to be less reactive to byproducts of the chemical processes [3]. A large amount of current research is devoted towards the development of solid electrolytes, to increase the safety of the batteries. The separators are made of cotton, nylon, glass, or ceramic materials for the selective movement of ions.

LIB's are examples of very complex chemical subsystem, and they have multiple phenomenon going on simultaneously [22]. Hence, measurement of the current state of the battery is not possible by any known means. Also, there are around tens of thousands of cells used in an automotive battery pack, and it would not be possible to measure the output states of each cell. Hence, there is a need of battery models and estimators that help us keep track over the operation of lithium-ion cells.

1.3 Modeling Approaches

The accurate modeling of batteries has gained importance with the same industry that pioneered the introduction of a high capacity LIB, portable electronics. Even in current smartphone industry, a major weighing factor is if the phone could make it through the day. Now, correct estimation of the state of charge (SOC) of the battery for the user feedback, and the battery life according to the current usage, are made based on the battery models. It becomes even more safety critical for automotive applications, because of the sheer energy of the battery packs.

However, for mobile applications, the battery models are constrained by the amount of processing power available onboard. This chapter summarizes a few approaches of modeling the batteries with increasing computational complexity.

1.3.1 Phenomenological Models

The name for these models comes from phenomena observation, i.e. empirical testing. The data recorded through the elaborate testing is fitted into models that could simulate the same behavior in an inexpensive way.

One example, the Equivalent Circuit Modeling (EQM) is a widespread technique used in electrical engineering to represent physical processes in form of a theoretical circuit. Starting with linear and passive elements, they could be used to represent non-linear behavior. A typical EQM battery model consists of a resistor to denote the internal resistance of the cell, voltage source to represent the open circuit voltage (OCV), and an RC circuit to capture to dynamic behavior of battery. The values for these elements are typically estimated by EIS

(electrochemical impedance spectroscopy) testing [23], [24]. Typically, these testing are carried out between frequencies of few Hz to 10 kHz for different state of charge states (and at times temperature).

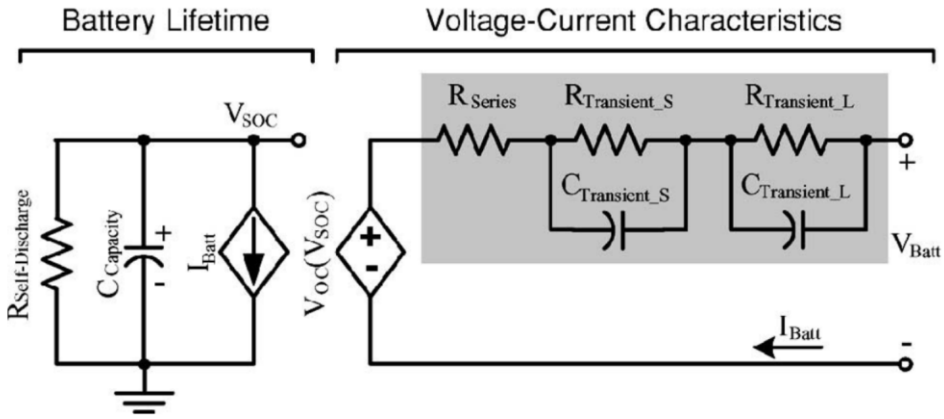

Figure 1-2 :EQM proposed by Chen [8]

Figure 1-2 shows a model proposed by Chen et al. [8] to represent the I-V characteristics of a polymer LIB. This model proposes an extra RC element where the R_{series} represents instantaneous voltage drop during a step response, "s" subsets represent the short time response like the exchange of charge and double electric effects, and "L" subsets are for long time response like the exchange of mass, i.e. lithium ions in the electrodes in the battery. All these parameters, including the V_{soc} are functions of SOC of the cell. However, the major contribution of the work is to present an equivalent circuit representation of the capacity fade. The capacitor, $C_{capacity}$, depends on the cycle number and the temperature of the cell, and there is a self-discharge resistor which represents the loss of charge while the battery is in standby.

Chen [8] reported an error of 0.4%, with a voltage response within 30mV error when the tests were done at a maximum of C/3 discharge rate where C is the rated capacity of the battery. With an increasing current requirement, the model would start to increasingly deviate with the results. These results represent the limits of accuracy the phenomenological models (i.e. models derived from empirical data) can reach. Physical models can reach a better accuracy because they try to understand the underlying physics of a battery.

1.3.2 PDE based Models

Partial differential equations or PDE's are the forerunners of the current development of mathematical science. They are pervasive in the field of physics, chemistry, and real sciences, and are used to model most of the real-life systems. Generally, the systems expressed by a set of PDE's have an infinite-dimensional configuration space, which makes them very difficult to solve. There are many methods of estimating the solutions to these equations, and there is

still a need of better optimization methods to solve these equations. However, let us come back to the topic at hand.

To first define the PDE's for the internal dynamics of the battery, we first need to identify different processes happening in the battery. The Figure 1-3 shows the stages of building a physics based model mentioned by Gregory Pelt [25].

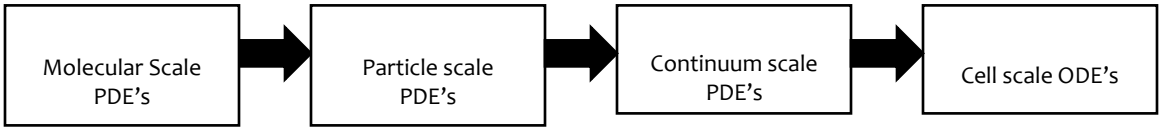

Figure 1-3 Development of physics-based models [25]

The process starts at an atomic level, where parameter values of diffusion rates of lithium in the electrodes are measured directly. The parameters of diffusivity, and open-circuit potentials would be used later in the full order physics-based models. At the particle scale, the expansion of molecular level into solid electrodes and electrolyte are made with an assumption of homogeneity. The model parameters for this scale like the porosity and tortuosity are measured in the laboratory.

The volume averaging of the particle scale model over the complete domain of a cell is deemed as continuum scale model. This model accommodates for the interaction of the solid and liquid regions and is referred as full-scale order model. The Figure 1-4 shows a representation of the PDE based continuum scale model.

Let us set the stage for the continuum theory model, or the PDE based model which has been worked through this thesis. As mentioned, the name porous electrode theory comes from the fact that the electrodes are geometrically porous matrices with a single reactive electronic conductor [19]. We define potentials Φ_s and Φ_e in solid and electrolyte respectively which are functions of time and space. The porosity of electrode ε is defined as the volume fraction of solid and electrolyte and the interfacial area is defined as the surface area of the pores per unit volume of the electrodes [19].

The flux density, *j*, is the wall flux of a species averaged over the interfacial area in the direction pointing towards the solution. This generates the Butler-Volmer equation that allows obtaining the current density, which could be found in the next chapter. The next equations in the PDE model are the mass balance equations and charge balance equation for the lithium-ion species in the solid and the liquid phase. The complete set of equations of the porous electrode theory can be found in Chapter 3.

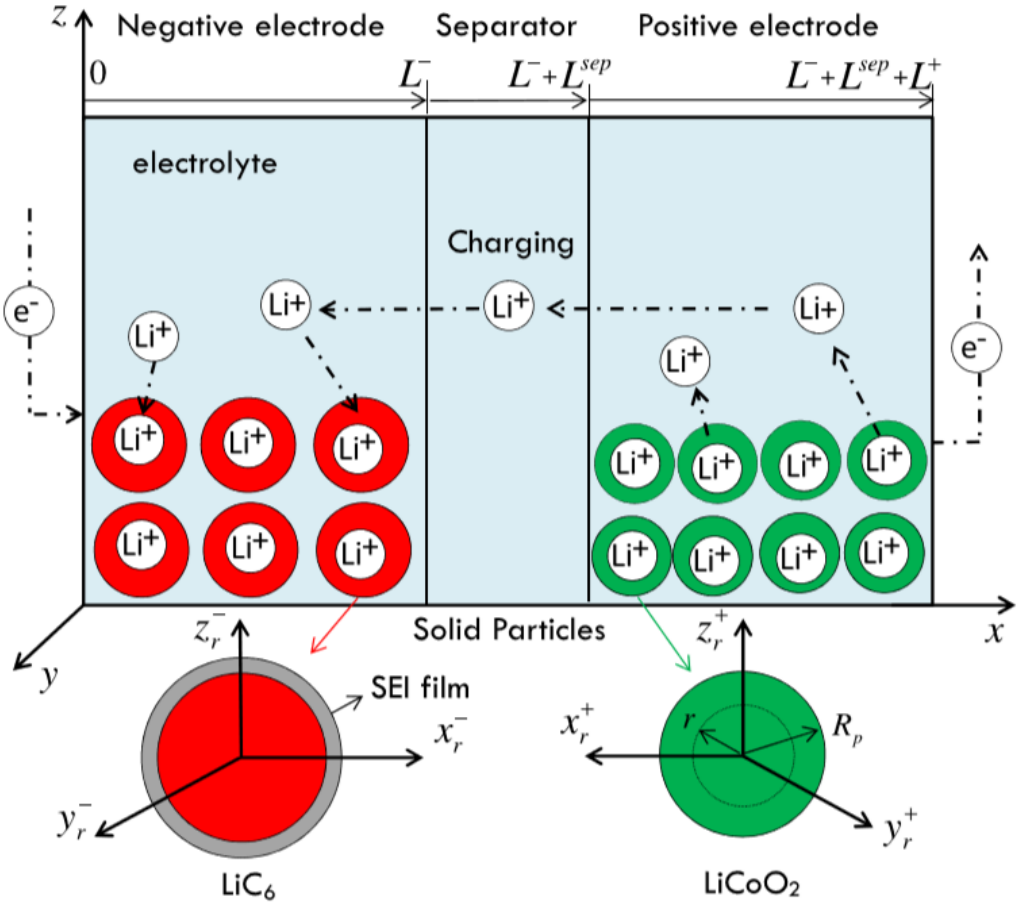

Figure 1-4 The co-ordinate system for a LIB reflecting physics-based models [26]

The final step of the modeling (into the mathematical realms) is to convert the set of PDE's into coupled ordinary differential equations, so that they could be used with inexpensive processors and mobile applications. The following Chapter 2 of the thesis talks about the state-space realization method using the Ho-Kalman method to reduce the equations.
There are other methods for reducing the set of partial differential equations, and work done by Zou et al. [26] could be summarized to explain the process of simplification using Hilbert space transformation. The initial set of PDE's selected for the reduction include the temperature, heat generation, and the aging equations, summarizing to a set of 17 PDEs. The Figure 1-5 reproduces the chart presented by Zhou in their work. The typical assumption for the first reductions is to assume that the time constant for electrical dynamics are faster than the mass movement time constants.

The methods of model reduction are be revisited in Chapter 5 of the thesis, but any new approaches to model reduction is out of the scope of the thesis. The following chapter introduces the development of few models as suggested by Gregory Plett [25].

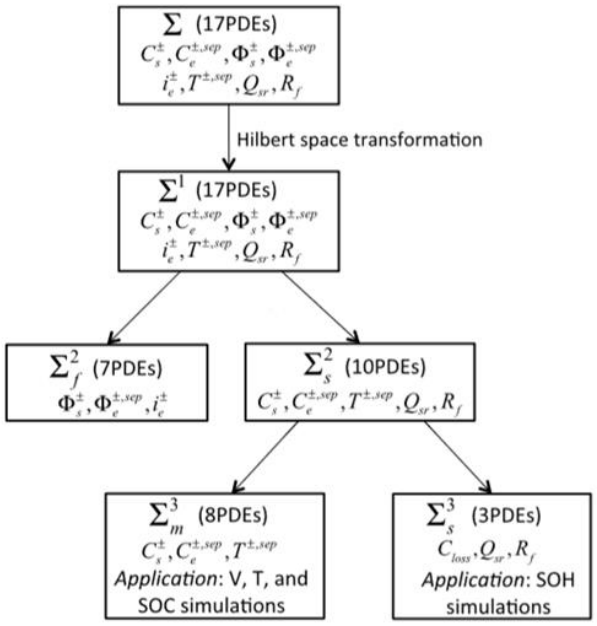

Figure 1-5 Framework for PDE reduction by Zou [26]

2 Developing physical models

2.1 Background

This chapter discusses implementation of three models based on the porous electrode theory as proposed by Newman and Doyle [27] – which would be discussed in more detail in the upcoming Chapter 3. It is necessary to point out that the model proposed by Newman to simulate a battery uses various other concepts to quantify different behaviors, ohm's law to express solid phase charge conservation, concentrated solution theory to express ionic transport in electrolyte, Butler-Volmer to express local current density, and finally the porous electrode theory to assume the electrodes as a lump of perfectly sized spheres to consider ion diffusion through solid gradients [28]. However, in current literature the whole model is referred in general as the porous electrode model.

The models developed in this chapter follow the lead by the book, Battery modeling by Gregory Pelt [25]. This chapter follows a gradual approach of reducing complexity starting from a 1-D implementation of the porous electrode model, to a reduced model of a set of 3 algebraic equations, in course reducing the complexity for suiting inexpensive computational resources. The computational complexity for the porous electrode theory is too high to be suitable for various applications[26], constrained by processing power, cost, and at times space. The assumptions made in each step will continually be mentioned in each section.

2.1.1 Pseudo 2D Model: COMSOL

Continuum refers to a type of modeling where there is continuous sequence of change in a quantity which may not be distinguishable with each other, but extremities are very different [25]. A continuum battery model would be a macroscale model which is made by averaging macroscopic quantities over a finite volume. It is called a pseudo 2D model, as the second dimension is the electrode particle radius to account for diffusion on the solid electrode (mass balance in the electrode), and basically works as a 1-D model.

However, the extra dimension in the pseudo 2D model causes a greater computational complexity [29], and most of the work in the current reduction literature is focused towards elimination of this spatial dimension.

The following equations summaries the modified porous electrode theory. The major assumptions for the model are as listed [26], [27].

- The whole battery domain is a macro-homogenous phase, the errors and particle irregularities are volume averaged, and hence, the electrode is made of homogenous spheres of same radii.
- The migration of ions and electrons are not caused by convection
- The electrolyte is diluted or ideal (the activity coefficient ==1)

The equations used for the model are briefly explained in the following section. For more detailed explanation of the equations, one could refer the work by Newman [19] and Smith [30].

a) Charge conservation in solid phase

$$\nabla \cdot \left(\sigma_{s,eff} \nabla \bar{\phi} s\right) = a_s F \bar{j} \qquad \text{Equation 1}$$

This equation states that the divergence of the current density at any volume in a cell is equal to the net charge arriving or exiting from that given volume. The first term indicates the current density like the ohm's law, as $\sigma_{s,eff}$ is the solid phase conductivity, $\bar{\phi}s$ is the solid phase potential. The a_s variable represents the interfacial area in final term, with j being the exchange current density and F the faraday constant, with a value of 96 485.3329 s A / mol.

The dash above the quantities mean that they are volume averaged quantities.

b) Mass conservation equation in Solid phase

This equation, known as the Fick's law of diffusion, signifies diffusion in a new spatial dimension of particle radius r that explains the rate of change of lithium concentration (c_s) at a localized volume. The assumptions are that the particle is completely spherical, and that the particle is centered at all locations in the electrode [25].

$$\frac{\partial c_s}{\partial t} = \frac{1}{r^2}\frac{\partial}{\partial r}\left(D_s r^2 \frac{\partial c_s}{\partial r}\right) \qquad \text{Equation 2}$$

c) Charge conservation in electrolyte phase

It uses the volume averaging theorem on the liquid phase charge conservation equation, stating the charge continuity equation in the electrolyte. It states that the net charge flux entering or exiting the electrolyte volume is equal to the divergence of current density (second term), and the logarithmic concentration gradient in the electrolyte.

$$\nabla \cdot \sigma_{s,eff} \nabla \phi s + \nabla \cdot \left(K_{eff} \nabla \phi e + K_{D,eff} \nabla ln \tilde{c}_e\right) + a_s F \bar{j} = 0 \qquad \text{Equation 3}$$

$$K_D = 2RTk(t_+^0 - 1) \qquad \text{Equation 4}$$

The K_{eff} term is the liquid phase conductivity, and K_{eff} represents the liquid state potential. The solid conductivity showing up in this equation represents the porous electrodes and the existence of homogenously distributed medium. The equation 4, expresses ionic conductivity K_D, as function of reaction rate and the transference number, t_+^0 that has been used in the final model in Chapter 5.

d) Mass conservation in the electrolyte phase of porous electrode

It states that the local vol-averaged concentration of lithium could change due to a concentration gradient depending upon the electrolyte diffusion flux, or if there is a local flux from solid to electrolyte, which depends on transference number.

$$\frac{\partial(\varepsilon_e \bar{c}_e)}{\partial t} = \nabla \cdot \left(D_{e,eff} \nabla \bar{c}_e\right) + a_s(1 - t_+^0)\bar{J} \qquad \text{Equation 5}$$

The parameter ε_e represents the electrolyte volume fraction, and $D_{e,eff}$ represents the diffusivity constant of the electrolyte medium.

e) Butler-Volmer Kinetics equation for the flux density of species

This equation represents to solid-electrolyte interface and uses the dependence of all intertwined parameters to help calculate the overall potential of the cell. The equation is discussed in detail in the upcoming chapters.

$$\bar{J} = j\left(\bar{c}_{s,e}, \bar{c}_e, \overline{\phi_s}, \overline{\phi_e}\right) \qquad \text{Equation 6}$$

2.1.2 State Space Reduction: MATLAB

Reduced order models work by reducing the complexity of continuously time-space varying partial differential equations by converting them into discrete time Ordinary Differential Equations (ODEs) via finding transfer functions. The 6 PDE's for charge, concentration, and potential for both electrodes and electrolyte domain will be modelled in MATLAB, by using the transfer functions, from the reference book [25]. The step by step reduction of solid-state dynamics is achieved, but rest of the equations are presented by the final deduced result.

a) Solid State Dynamics

This equation 7, of the solid diffusion will be reduced by the approach suggested by the Jacobsen and West [25], [31].

$$\frac{\partial c_s(r,t)}{\partial t} = \frac{1}{r^2}\frac{\partial}{\partial r}\left(D_s r^2 \frac{\partial c_s(r,t)}{\partial r}\right) \qquad \text{Equation 7}$$

The boundary conditions can be given by

$$Ds\frac{\partial c_s(0,t)}{\partial r} = 0, Ds\frac{\partial c_s(R_s,t)}{\partial r} = -j(t) \qquad \text{Equation 8}$$

With initial concentration, $c_s(r,0) = c_{s,0}$, $\beta(r) = r\sqrt{s\,/\,D_s}$, and an assumption of the D_s to be constant, we reach the transfer function,

$$\frac{\widetilde{C_s}(r,s)}{J(s)} = \frac{-R_s^2}{D_s r}\left(\frac{e^{\beta(r)} - e^{(-\beta(r))}}{(1-\beta(R_s))e^{\beta(R_s)} - (1+\beta(R_s))e^{-\beta(R_s)}}\right) \qquad \text{Equation 9}$$

Reducing for the surface concentration, we have,

$$\frac{\widetilde{C_s}(R_s,s)}{J(s)} = \frac{R_s}{D_s}\left(\frac{1}{(1-\beta(R_s)\coth(\beta(R_s)))}\right) \quad \text{Equation 10}$$

As we see, we have an integrator pole at s=0, we will create a debiased variable (also known as tilde notation), by subtracting the average quantity, which in this case, is concentration.

$$\frac{\Delta\tilde{C}_{s,e}(s)}{J(s)} = \frac{R_5}{D_s}\left[\frac{(\beta^2+3)-3\beta\coth(\beta)}{\beta^2(1-\beta\coth(\beta))}\right] = \frac{s\frac{R_s^2}{D_s}+3-3R_s{}^2\sqrt{\frac{s}{D_s}}\coth(R_s{}^2\sqrt{\frac{s}{D_s}})}{sR_s(1-R_s{}^2\sqrt{\frac{s}{D_s}}\coth(R_s{}^2\sqrt{\frac{s}{D_s}})} \quad \text{Equation 11}$$

Where we have,

$$\frac{\Delta\tilde{C}_{avg}(s)}{J(s)} = \frac{-res_0}{s} = \frac{=3/R_s}{s} \quad \text{Equation 12}$$

This model still yields the value of transfer function to infinity after it's zero, so we use L'Hospitals rule to calculate the lim s-> 0 on equation 11, multiple times to get the value at s=0. This limit can be calculated using a limit function in my MATLAB code.

The transfer functions are the first step to write the 1D reduced order model. It follows by the creating of DRAs, and then the system could be used for predicting the internal parameters. Below are the different transfer functions which have been modeled [25]. Following steps are involved in generating the discrete equation [25].

Pre-step: Compute the bode magnitude plot for our transfer function to estimate the bandwidth and choose an appropriate sampling rate. It is a recognized format for finding frequency response of time variant systems. The x axis is logarithmic denoting frequency and the x axis has phase in degrees and magnitude in decibels.

Step1: Sampling the transfer function at discrete frequencies and drafting approximate continuous-time impulse response with inverse DFT (Direct Fourier Transform, computed using the ifft command in MATLAB).

Step2: Cumulating the discrete values to find out the continuous time step response.

Step 3: Resample the results for the desired sample time, for example 1 sec, and compute discrete time pulse response.

Step 4: Use the discrete time pulse response to find out the step-space realization by the deterministic Ho-Kalman algorithm. The algorithm starts with creating two squares Hankel Matrices, imposing Single Value decomposition to determine the order of the system, and then compute the system of matrices to define the system.

Table 1 : Transfer Functions for the State space reduction model [25]

Neg Current flux density	-J_{neg}	$\frac{I^{neg}(z,s)}{I_{app}(s)} = v^{neg}(s)\frac{\sigma_{eff}^{neg}\cosh(v^{neg}(s)z)+k_{eff}^{neg}\cos h(v^{neg}(z-1))}{a_s^{neg}FL^{neg}A\left(k_{eff}^{neg}+\sigma_{eff}^{neg}\right)\sinh(v^{neg}(s))}$
Surface potential	$\tilde{\phi}_{s-e}^{neg}$	$\frac{\tilde{\phi}_{s-e}^{neg}(z,s)}{I_{app}(s)} = \frac{L^{neg}(\sigma_{eff}^{neg}\cosh(v^{neg}(s)z)+k_{eff}^{neg}\cos h(v^{neg}(z-1)))}{A\sigma_{eff}^{neg}k_{eff}^{neg}v^{neg}(s)\,sinh(v^{neg}(s))}, \frac{[\tilde{\phi}_{s-e}^{neg}(z,s)]^*}{I_{app}(s)} = \frac{\tilde{\phi}_{s-e}^{neg}(z,s)}{I_{app}(s)} + \frac{1}{\varepsilon_s^{neg}AFL^{neg}s}\left[\frac{\partial U_{ocp}}{-\partial c_{s,e}}\Big\|_{C_{s,0}}\right]$
Neg Surface concentration	– c_{neg}	$\frac{\tilde{c}_{s,e}^{neg}(z,s)}{I_{app}(s)} = \frac{\sigma_{eff}^{neg}\cosh(v^{neg}(s)z)+k_{eff}^{neg}\cos h(v^{neg}(z-1))}{a_s^{neg}FL^{neg}A\left(k_{eff}^{neg}+\sigma_{eff}^{neg}\right)\sinh(v^{neg}(s))}\frac{R_s^{neg}{}_*v^{neg}(s)}{1-R_s^{neg}\sqrt{s/D_s^{neg}}\coth\left(R_s^{neg}\sqrt{s/D_s^{neg}}\right)}, \frac{[\tilde{c}_{s,e}^{neg}(z,s)]^x}{I_{app}(s)} = \frac{\tilde{c}_{s,e}^{neg}(z,s)}{I_{app}(s)} + \frac{1}{\varepsilon_s^{neg}AFL^{neg}s}$
Neg Solid potential	-$\tilde{\phi}_s^{neg}(z,s)$	$\frac{[\tilde{\phi}_s^{neg}(z,s)]}{I_{app}(s)} = -L^{neg}\left[\frac{K_{eff}^{neg}(\cos h(v^{neg}(s)-\cosh((z-1)v^{neg}(s)))+\sigma_{eff}^{neg}(1-\cosh(zv^{neg}(s))+zv^{neg}(s)\sinh(v^{neg}(s))}{A\sigma_{eff}^{neg}(k_{eff}^{neg}+\sigma_{eff}^{neg})v^{neg}(s)\sinh(v^{neg}(s)))}\right]$
Pos Solid potential	$\tilde{\phi}_{s-e}^{pos}(z,s)$	$\frac{\tilde{\phi}_{s-e}^{pos}(z,s)}{I_{app}(s)} = -\frac{L^{pos}(\sigma_{eff}^{pos}\cosh(v^{pos}(s)z)+k_{eff}^{pos}\cos h(v^{pos}(z-1)))}{A\sigma_{eff}^{pos}k_{eff}^{pos}v^{pos}(s)\,sinh(v^{pos}(s))}$
Concentration of the electrolyte	$c_e(x,t)$	$\frac{\tilde{c_e}(x,s)}{I_{app}(s)} = \sum_{n=1}\frac{\tilde{c}_{e,n(s)}}{I_{app}(s)}\Psi(x;\lambda_n), \frac{\tilde{c}_{e,n(s)}}{I_{app}(s)} = \frac{1}{s+\lambda_n}\left[\frac{J_n^{neg}(s)}{I_{app}(s)} + \frac{J_n^{pos}(s)}{I_{app}(s)}\right]$, Jneg and Jpos [25]
Electrolyte Potential	$\overline{\phi_e}(x,s)$	Negative electrode $\frac{\tilde{\phi}_e(x,s)]_1}{I_{app}(s)} = -\left[\frac{L^{neg}\sigma_{eff}^{neg}(\cosh\left(\frac{x}{L^{neg}}v^{neg}(s)\right)-1)+L^{neg}k_{eff}^{neg}(\cosh\left(\frac{(L^{neg}-x)}{L^{neg}}v^{neg}(s)\right)-\cosh(v^{neg}(s))}{Ak_{eff}^{neg}\left(k_{eff}^{neg}+\sigma_{eff}^{neg}\right)v^{neg}(s)\sinh(v^{neg}(s))}\right]-\frac{x}{A\left(k_{eff}^{neg}+\sigma_{eff}^{neg}\right)}$ Negative-electrode-separator Boundary $\frac{\tilde{\phi}_e(L^{neg},s)]_1}{I_{app}(s)} = -\frac{L^{neg}\left(\left(\sigma_{eff}^{neg}-k_{eff}^{neg}\right)\tanh\left(\frac{v^{neg}(s)}{2}\right)\right)}{Ak_{eff}^{neg}(k_{eff}^{neg}+\sigma_{eff}^{neg})(v^{neg}(s))}-\frac{L^{neg}}{A(k_{eff}^{neg}+\sigma_{eff}^{neg})}$ Separator $\frac{\tilde{\phi}_e(x,s)]_1}{I_{app}(s)} = -\frac{L^{neg}\left(\left(\sigma_{eff}^{neg}-k_{eff}^{neg}\right)\tanh\left(\frac{v^{neg}(s)}{2}\right)\right)}{Ak_{eff}^{neg}(k_{eff}^{neg}+\sigma_{eff}^{neg})(v^{neg}(s))}-\frac{L^{neg}}{A(k_{eff}^{neg}+\sigma_{eff}^{neg})}-\frac{x-L^{neg}}{A(k_{eff}^{neg})}$ Separator-positive-electrode Boundary $\frac{\tilde{\phi}_e(L^{neg}+L^{sep},s)]_1}{I_{app}(s)} = -\frac{L^{neg}\left(\left(\sigma_{eff}^{neg}-k_{eff}^{neg}\right)\tanh\left(\frac{v^{neg}(s)}{2}\right)\right)}{Ak_{eff}^{neg}(k_{eff}^{neg}+\sigma_{eff}^{neg})(v^{neg}(s))}-\frac{L^{neg}}{A(k_{eff}^{neg}+\sigma_{eff}^{neg})}-\frac{L^{sep}}{A(k_{eff}^{sep})}$ Positive-electrode $\frac{\tilde{\phi}_e(x,s)]_1}{I_{app}(s)} = -\frac{L^{neg}\left(\left(\sigma_{eff}^{neg}-k_{eff}^{neg}\right)\tanh\left(\frac{v^{neg}(s)}{2}\right)\right)}{Ak_{eff}^{neg}(k_{eff}^{neg}+\sigma_{eff}^{neg})(v^{neg}(s))}-\frac{L^{neg}}{A\left(k_{eff}^{neg}+\sigma_{eff}^{neg}\right)}-\frac{L^{sep}}{A\left(k_{eff}^{sep}\right)}-$ $\frac{L^{pos}(1-\cosh\left(\frac{(L^{neg}+L^{sep}-x)}{L^{pos}}v^{pos}(s)\right)-L^{pos}\sigma_{eff}^{pos}(\cosh(v^{pos}(s))-\cosh\left(\frac{(L^{tot}-x)}{L^{pos}}v^{neg}(s)\right)}{Ak_{eff}^{neg}(k_{eff}^{neg}+\sigma_{eff}^{neg})(v^{neg}(s))\sinh(v^{neg}(s))}-\frac{(x-L^{neg}-L^{sep})}{A(k_{eff}^{pos}+\sigma_{eff}^{pos})}$ At the cell Boundary $\frac{[\tilde{\phi}_e(x,s)]_1}{I_{app}(s)} = -\frac{L^{neg}\left(\left(\sigma_{eff}^{neg}-k_{eff}^{neg}\right)\tanh\left(\frac{v^{neg}(s)}{2}\right)\right)}{Ak_{eff}^{neg}(k_{eff}^{neg}+\sigma_{eff}^{neg})(v^{neg}(s))}-\frac{L^{neg}}{A\left(k_{eff}^{neg}+\sigma_{eff}^{neg}\right)}-\frac{L^{sep}}{A\left(k_{eff}^{sep}\right)}-\frac{L^{pos}\left(\left(\sigma_{eff}^{pos}-k_{eff}^{pos}\right)\tanh\left(\frac{v^{pos}(s)}{2}\right)\right)}{Ak_{eff}^{pos}(k_{eff}^{pos}+\sigma_{eff}^{pos})(v^{pos}(s))}-\frac{L^{pos}}{A\left(k_{eff}^{pos}+\sigma_{eff}^{pos}\right)}$
Cell voltage Computation	$v(t)$	$n^{pos}(z,t) = \frac{2RT}{F}asin\,h\left(\frac{j^{pos}(z,t)}{2k_0^{pos}\sqrt{c_e(z,t)(c_{s,max}^{pos}-c_{s,e}^{pos}(z,t))c_{s,e}^{pos}(z,t)}}\right)$ $v(t) = F\left(R_{film}^{pos}j^{pos}(0,t) - R_{film}^{neg}j^{pos}(0,t)\right] + [\tilde{\phi}_e(L^{tot},t)]_1 + [n^{pos}(0,t) - n^{neg}(0,t)] + [\tilde{\phi}_e(L^{tot},t)]_2 + \left[U_{ocp}^{pos}\left(c_{s,e}^{pos}(0,t)\right) - U_{ocp}^{neg}\left(c_{s,e}^{neg}(0,t)\right)\right]$

From here, the transfer functions could be decomposed using the steps mentioned above. v can be interpreted as the ratio of the frequency dependent and SOC dependent impedances. It is of importance as it repeats itself in most of the equations. Table 1 summarizes the transfer functions for the various state variables used in the model.

$$v^{neg}(s) = \frac{L^{neg\,2}\sqrt{\frac{a_s^{neg}}{\sigma_{eff}^{neg}}+\frac{a_s^{neg}}{k_{eff}^{neg}}}}{\sqrt{R_{s,e}^{neg}+\frac{R_s^{neg}}{FDs^{neg}}\left[\frac{\partial U_{OCP}^{neg}}{\partial C_{s,e}^{neg}}\right|_{C_{s,0}^{neg}}]\left[\frac{1}{1-R_s^{neg}\sqrt{s/D_s^{neg}}\coth\left(R_s^{neg}\sqrt{s/D_s^{neg}}\right)}\right]}} \quad \text{Equation 13}$$

2.1.3 Single Particle Model: Simulink

The complexity of these models has been driving the work towards the reduction of PDEs into algebraic differential equations, and this model uses the work by Venkat et al. [32] and Venkatasailanathan et al. [33]. They reduced the microscale solid phase mass conservation equation, the Fick's law of diffusion, into a set of three differential equations. The known assumption is that the solid-state concentration inside the spherical particle can be expressed as a polynomial in the spatial direction.

$$c(r,t) = a(t) + b(t)\left(\frac{r^2}{R_p^2}\right) \quad \text{Equation 14}$$

In this MATLAB model the flux concentration has not been implemented, unlike Venkat et al. [32] so it takes it even farther from generating an actual battery configuration. So, it is essentially reducing the 3-algebraic equation single particle model to a surface concentration-based model with 2 algebraic equations. The following equations have been replicated from [4] with a few modifications and have been used in the model.

$$j_n = \frac{I}{F*a_s*A*L} \quad \text{Equation 15}$$

$$\frac{dc_s}{dt} = -3\frac{j_n}{R_p} \quad (reduced) \quad \text{Equation 16}$$

$$c_{ss} = c_s - \frac{R_p}{D_s}j_n \quad (reduced) \quad \text{Equation 17}$$

$$\theta = \frac{2RT}{F}\sin\hbar^{-1}[\frac{I}{2aLr_{eff}\sqrt{c_c^0 c_{ss}(c_{s,max}-c_{ss})}}] + U(c_{ss}) + \frac{R_f I}{a\,L} \quad \text{Equation 18}$$

It is not a common practice by manufacturers give the reaction rate constant for batteries, hence, the input values for the k_{onorm}, the normalized reaction rate coefficient, and Reaction rate, r_{eff} were calculated by using the following equation,

$$r_{eff} = k_{0,norm}/(ce0^{0.5}c_{s,max}) \quad \text{Equation 19}$$

The equations for the open circuit potentials for the LFP and LIC6 were taken from work by Zou. [26] The plots are shown in Figure 2-1.

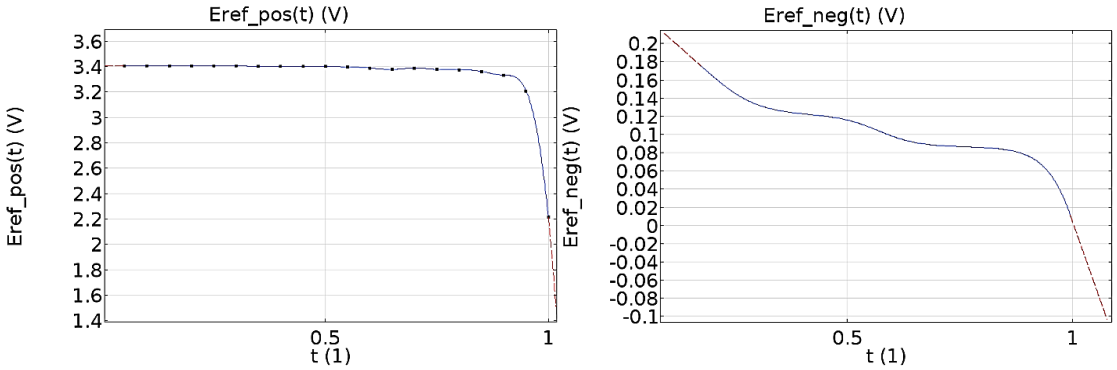

Figure 2-1: Open circuit potentials of electrodes

$$U_{LFP} = 2.567462 + 57{:}69[1 - \tanh(100z + 2.9163927) + 0.442953 \tan - 1(-65{:}41928z + 64{:}89741)0.097237 \tan - 1(-160.9058\,z + 154.590)$$ Equation 20

$$U_{LiC6} = 0.6379 + 0{:}5416 \exp(-305.5309z) + 0.044\tanh[-(z - 0.1958)/0.1088) - 0.1978 \tanh[(z - 1.0571)/0.0854] - 0.6875 \tanh[(z + 0.0117)/0{:}0529] - 0.0175 \tanh[(z - 0.5692)/0{:}0875]$$ Equation 21

These are the standard voltages of electrodes against the concentration of lithium ion. For the final prediction of voltages, we need the over potential curve, along with this plot to predict the cell voltage.

2.2 Comparison and Results

This section compares results generated by the three models. Due to limitations of different models to generate different state variables, only selected comparisons are made between different models. The current testing waveform has been extracted from an electric motorcycle drive-cycle, where a current profile of 1728 seconds is being utilized, as shown in Figure 2-2.

The maximum current discharge has been noted at a time stamp of 1409 seconds, which corresponds to a value of 2.13 amps. This time stamp has been used to record values for comparison, and another time stamp of 1539, when a negative current of 0.324 amps is supplied to the battery.

2.2.1 Cell Voltage

COMSOL: The simulation starts with the battery at SOC of 45%, and the manufacturer reported nominal voltage is 3.3 V. The cell voltage profile has been recorded in Figure 2-3.

This plot is mostly straight forward, the results generated seem to be in sync with the manufacturer claims. The main take away from this plot is the dynamic behavior and the

voltage drop observed at the peak current values. It would be interesting to compare this data to an experimentally observed data to find out the accuracy of COMSOL model.

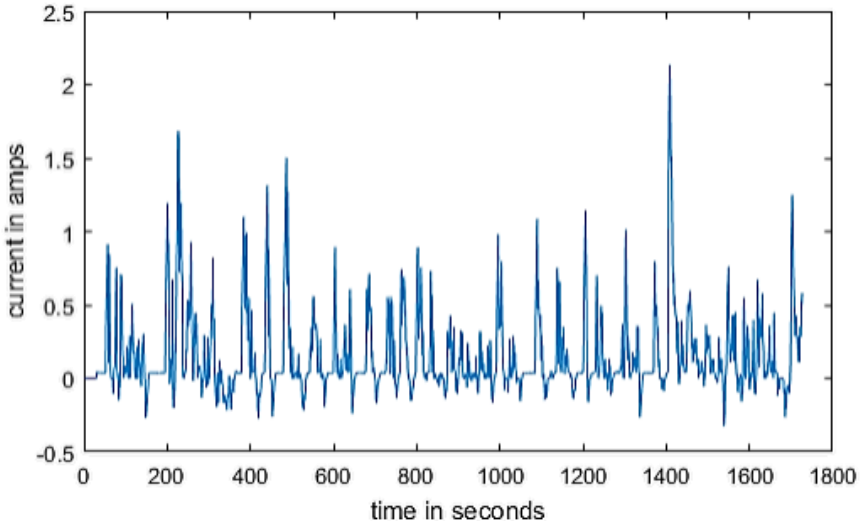

Figure 2-2: Current Profile being tested

SPM: There are numerous differences occurring in the voltage profiles, the equilibrium voltages reported are offset by a value of 0.07V. Also, the voltage reported in SPM follows a decreasing trend with the SOC loss, which is not evident in the COMSOL model.

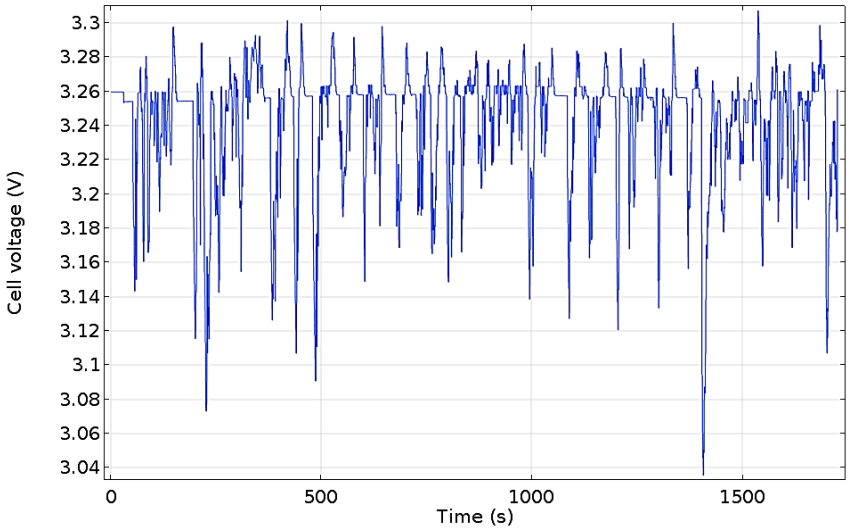

Figure 2-3: Voltage profile with COMSOL Model

The dynamic peaks in COMSOL model are in the same order as in the SPM model, but during the peak current of 2.1 Amps, the SPM voltage drops by 0.7 volts which is an unrealistic number for a 3.3Ah battery. The SPM model is not supposed to work with high discharge currents as mentioned in the assumptions while formulating the model.

This is mostly the extent of results which could be drawn from the 2-equation SPM model, and they are not very satisfactory.

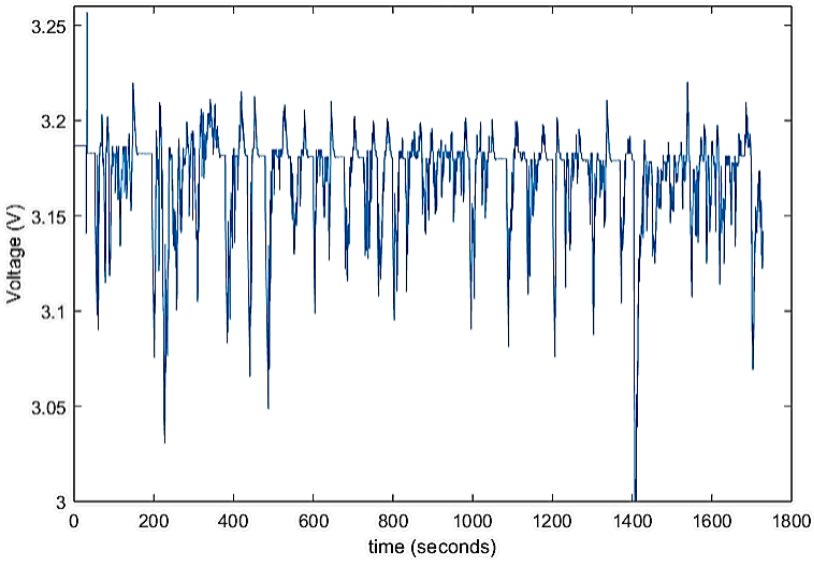

Figure 2-4: Voltage Profile SPM Model

2.2.2 Intercalation Flux

COMSOL: Figure 2-5 represents the varying flux with respect to the normalized length of the battery, where the three sections represent negative, separator, and the positive electrode starting from the left to right.

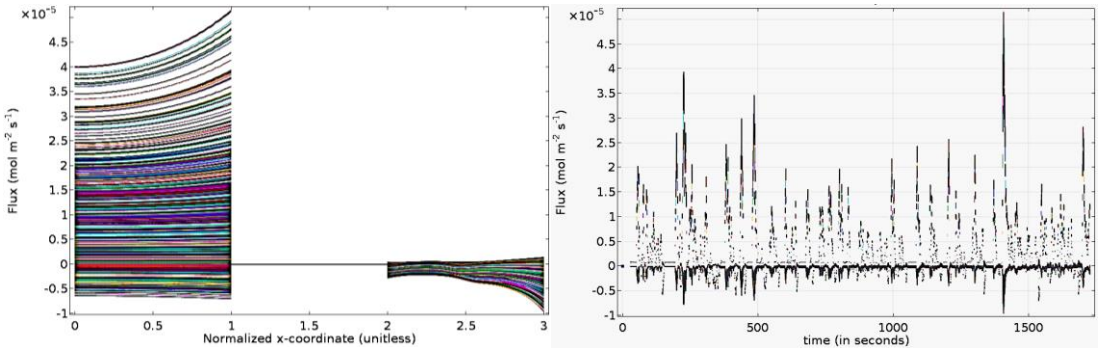

Figure 2-5: Intercalation Flux with normalized battery length and time in COMSOL Model

A current requirement causes a positive flux at the negative electrode, and vice-versa. However, the interesting observation here is that as the current requirement increases, the flux concentration starts to follow a curve path, as compared to a straight one.

The peak current requirements show that the negative flux at separator side is higher as compared to the current collector interface, in contrary to the positive electrode which follows an opposite trend. This can be explained by looking at the flux equation.

$$J = k_0^{norm}\left(\left(\frac{Ce}{Ce,0}\right)\left(\frac{C_{s,max}-C_{S,e}}{C_{s,max}}\right)\right)^{1-\alpha}\cdot\left\{e^{\left(\frac{(1-\alpha)F}{RT}\eta\right)} - e^{\left(\frac{(-\alpha)F}{RT}\eta\right)}\right\} \qquad \text{Equation 22}$$

As we will see in the future results, c_e rather increases at the collector ends so it couldn't be contributing to the decrease. As the overpotential is inter-related to flux, the cause is probably the drop of overpotential at the ends due to an outward flow of electrons. The independent nature also explains the parabolic nature of the curve.

The selected time stamps for highest discharge and a negative current have been recorded in Figure 2-6. We can also plot the flux densities with respect to time, however, all the values for different localized locations have been plotted simultaneously, which makes this graph difficult to comprehend, and directly compare.

Depending upon the current profile, and dynamics, there are a lot of variations captured in the COMSOL model, which couldn't be expected from the SPM model.

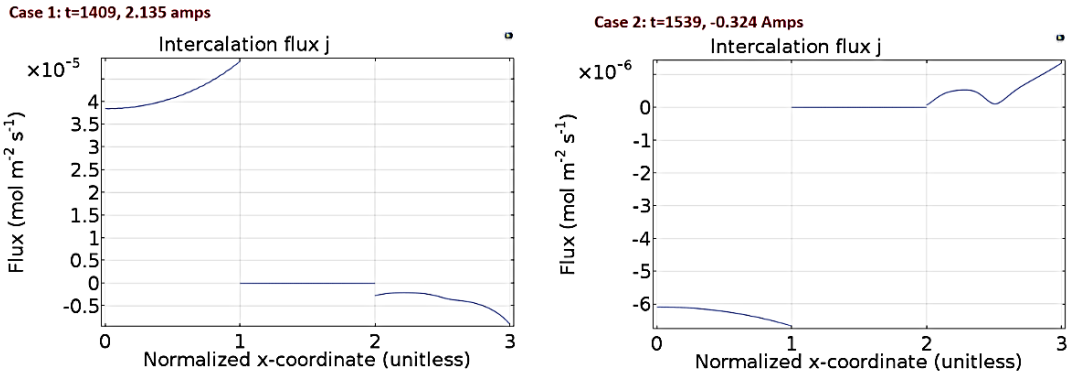

Figure 2-6 : Intercalation Flux, j with normalized battery length at selected time instances

SPM: The flux densities for the negative and positive electrode are shown in the Figure 2-7.

By comparing the maximum values of flux, the order of the flux densities for both the electrodes is the same as compared to the COMSOL model. However, this model does not consider the concentration fluxes, overpotential for calculating the flux, but it is a rather simple calculation of the oncoming current divided by the volumes of the electrode. (A/m^2)

It would not be great idea to compare the results from COMSOL model peaks with these results, as this is a rather averaged value, as compared to localized results plotted against time.

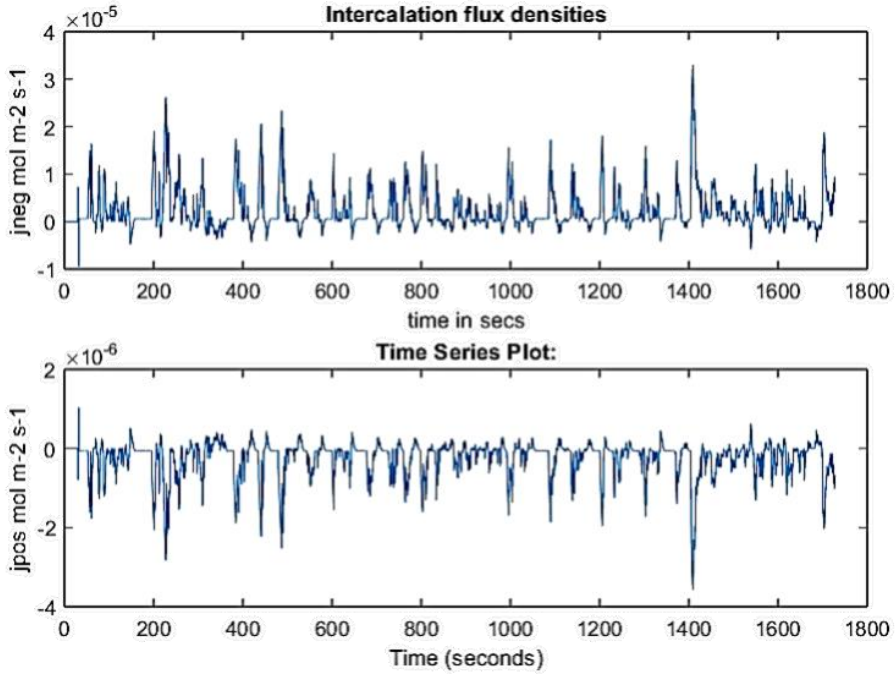

Figure 2-7: Intercalation flux with respect to time of the SPM model

2.2.3 Electrolyte Potential

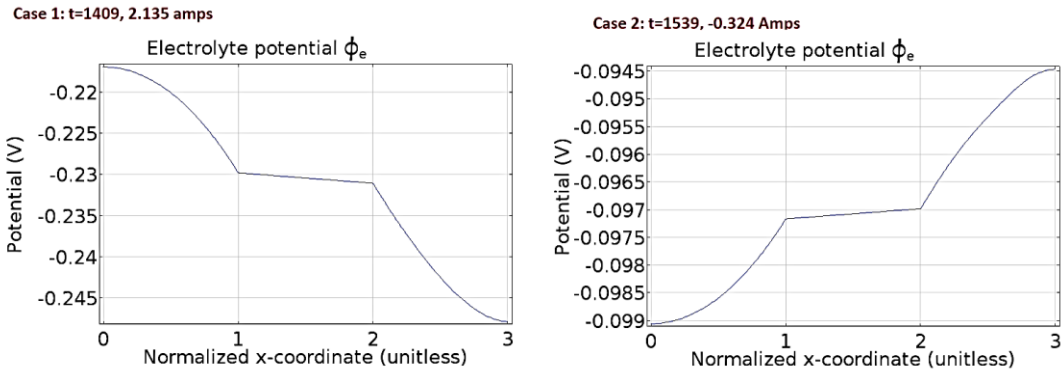

Figure 2-8: Electrolyte potential at Specific timestamps

COMSOL: At equilibrium, that is the beginning of the cycle, the potential across the electrolyte is distributed evenly across the normalized length to be -0.12 V. From the results plotted in the Figure 2-8, we can see that the electrolyte potential is a very dynamic parameter, and the potential flips readily with the application of an external current.

For a positive discharge rate - the negative electrode is at a higher potential- the electrolyte has a higher potential towards the negative electrode.

2.2.4 Electrolyte Concentration

COMSOL: We already used the electrolyte concentration results to predict if the trends got for the intercalation flux were reasonable. It turns out that the electrolyte concentration is an equally dynamic parameter like electrolyte potential. As the potential in electrolyte does depend on the concentration flux, it is easier to predict that the waveforms would be similar.

However, we can see in the plot for the time stamp 1539 (Figure 2-10), that the electrolyte concentration at the positive electrode struggles to keep up with the potential, as the current changes the direction to negative, in comparison to the negative electrode which has a smoother waveform. It could be argued that be the big particle size at the positive electrode makes dynamics slower.

Also, the electrolyte concentration at the separator keeps to the initial value of ce_0 which slight variations, which shows that there is no net increase in the concentration of the electrolyte while discharging and charging.

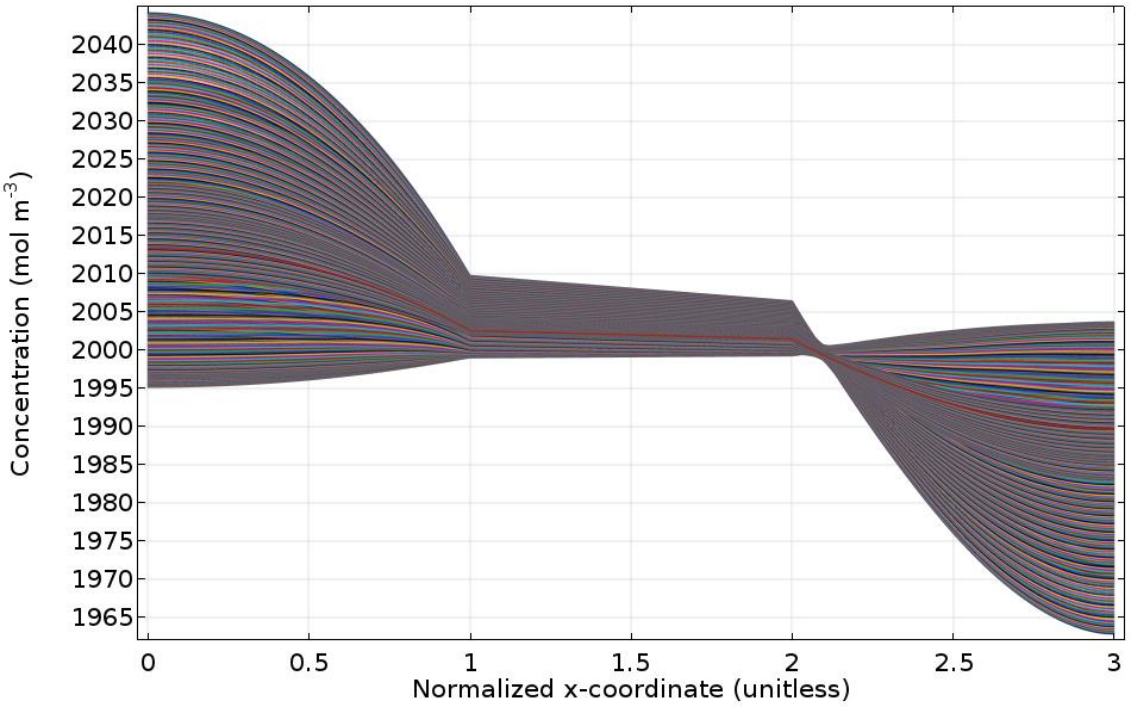

Figure 2-9: Electrolyte concentration as a function of normalized x-coordinates

State space DRA model: The reduced order model uses eigenvalues-based solution to calculate the electrolyte concentration, and it is only feasible to see the results at specific time instants. We have already calculated the results for time instants of max charge and discharge, and we could plot them to compare both.

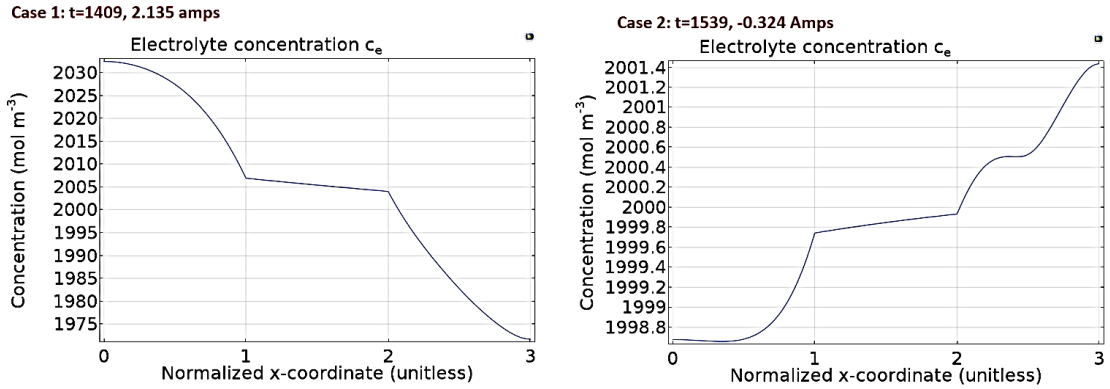

Figure 2-10: Electrolyte concentration at time stamps

The number of eigenvalues selected for plotting the Figure 2-11 below has been taken as 6. It is reported that increasing number of eigenvalues gets closer results to experimental data, however, increasing number of eigenvalues exponentially increases the time taken in simulation, which will be discussed later in the document.

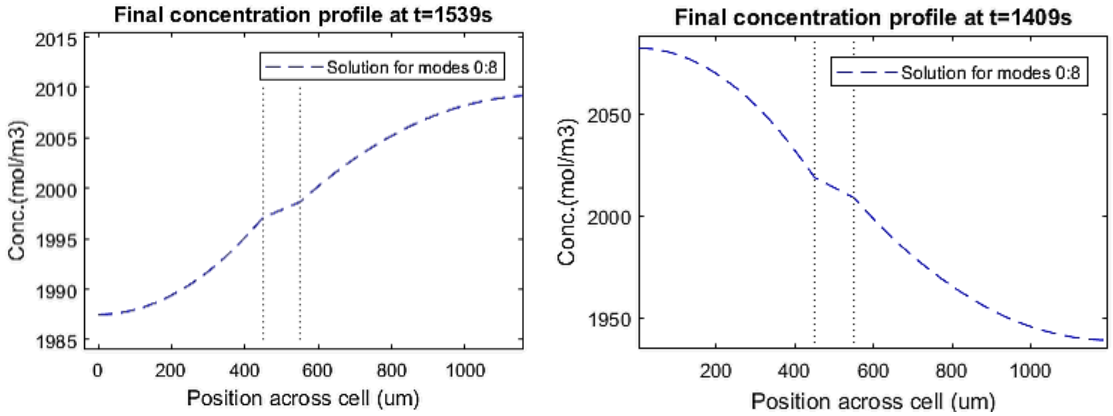

Figure 2-11: Electrolyte concentration at selected time stamps: state space model

In the case of a lower discharge rate of 0.324 amps, the concentration profile at the current collector interface fails short by a factor of 0.98, and at a higher discharge rate of 2.1 amps, the overshoot is higher by a factor of 1.07, although the potential at the separator interface is predicted right by the model. However, the intricacies in the dynamics is not predicted by the reduced order model, as it doesn't consider the previous current waveforms, rather a static value of current.

Figure 2-12 shows the comparison the results for different eigenvalues to present the deviation. The eigenvalues of 8 indeed is closer to the nature of the COMSOL generated result.

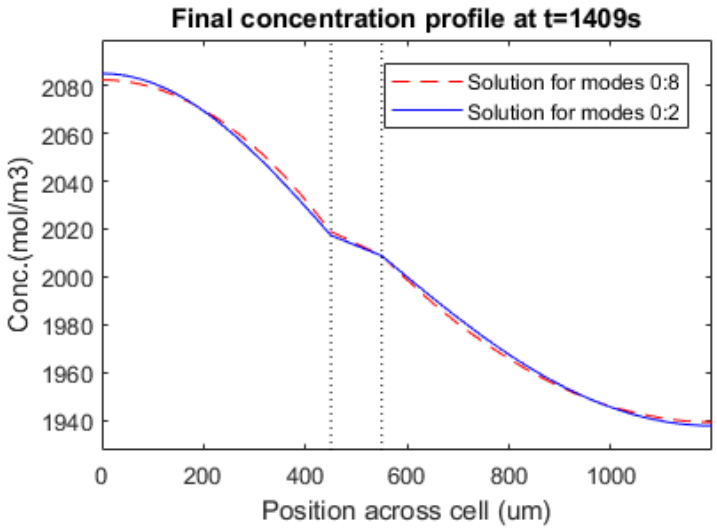

Figure 2-12: Comparison between different numbers of eigen values

2.2.5 Solid electrode concentration

COMSOL: The dynamics for solid surface concentration is a slow phenomenon in a battery, and it is the reaction which limits the charging and discharging rates of a battery. In the beginning they have flat concentrations divided equally at all locations of the electrodes. The lower curves represent the concentrations for the negative electrode, and the upper profile represents the concentration for positive electrode.

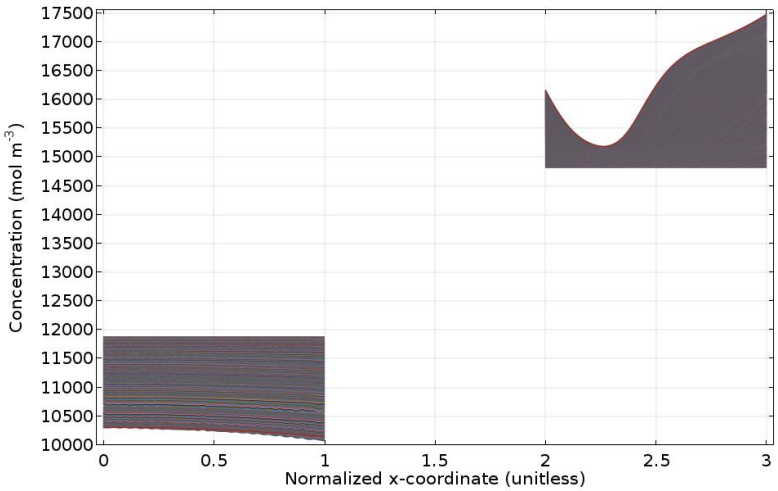

Figure 2-13: Solid Surface Concentration in the electrode: COMSOL

We can observe in the Figure 2-13 and 2-14 the dynamic difference of the concentration profiles for the positive and the negative electrode. The negative electrode has a uniform distribution of the concentration along the length, however, for the positive electrode, most of the lithium concentration is accumulated at the collector, and another localized high concentration is at

the separator interface. This agrees with existing literatures [28] adding validation to the model. This uneven distribution of ion concentration in positive electrode increases with increase in the discharge rate, and hence the consumption of positive electrode material is highly limited.

The same behavior can also be observed in the solid concentration vs time plot in Figure 2-14, where we can see that the positive electrode has a wide area of plots because of the different localized lithium ion concentrations, as compared to negative electrode which has rather consistent decrease in SOC.

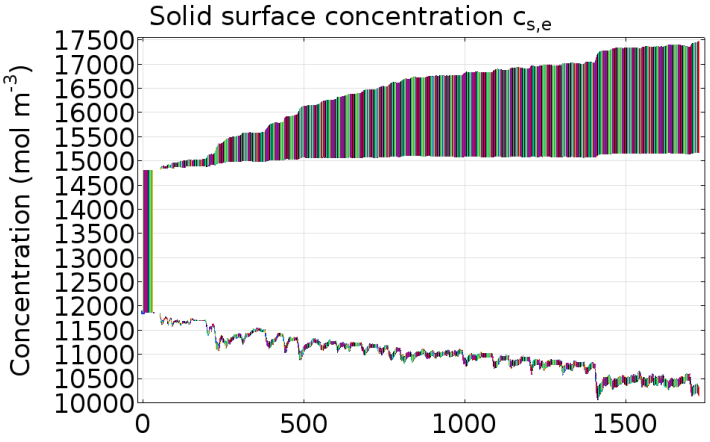

Figure 2-14: Electrode concentration with respect to time: COMSOL

SPM: These localized results cannot be generated from the SPM model, hence results in Figure 2-15 reports an averaged value of the concentrations.

The averaged final negative electrode concentration reported by COMSOL was around 10300 mol/m3, as compared to the result in SPM model with around 10800 mol/m3 concentration left to be used. Even for a period of 1800 seconds, this gap cannot be ignored.

State space: The first result shown in the Figure 2-16 is for the solid surface concentrations for the negative and positive electrode. The results are like the ones generated by the previous model, we can see if the plots with respect to localized locations could be made.

The result here seems to agree more with the continuum model, the positive densities didn't seem to vary as the negative concentration densities. This is probably because the intercalation rate at the LFP electrode is not as fast as compared to the Li metal negative electrode. The SPM model however, doesn't differentiate between the concentration profiles for the both electrodes, and are basically reciprocal to each other.

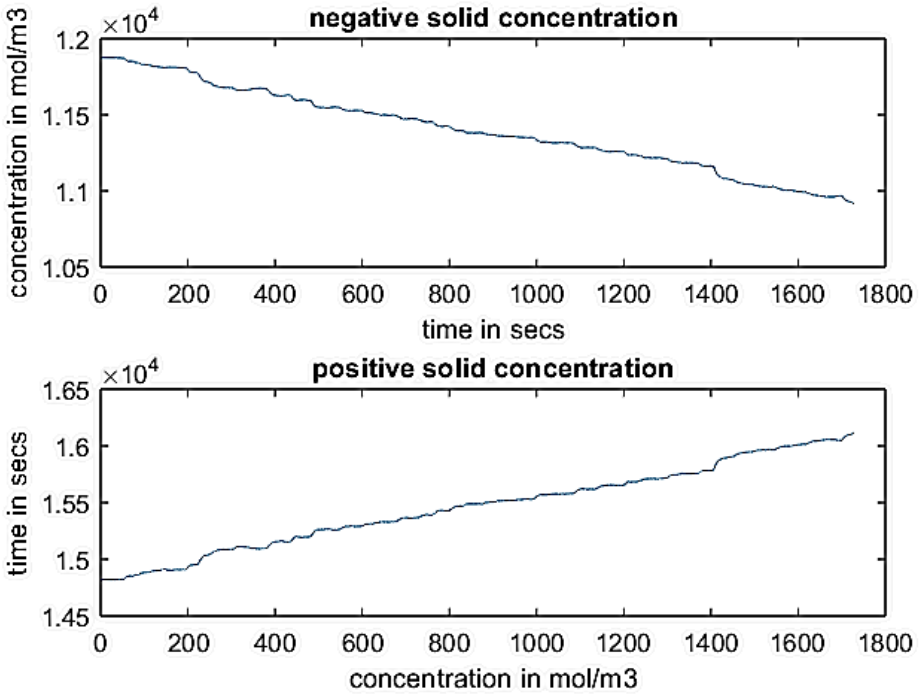

Figure 2-15: The Electrode concentrations

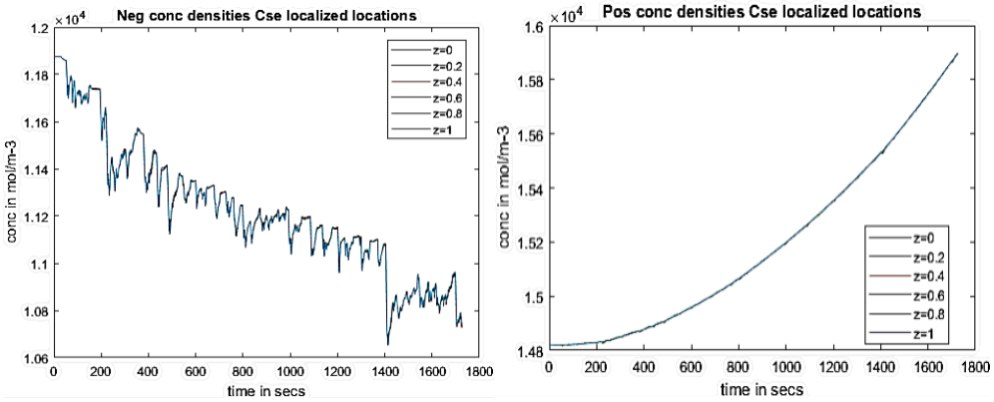

Figure 2-16: Solid concentration Profiles: State Space Model

2.3 Limitations and further approach

Each model has its own advantages and disadvantages and is better suited to different applications. The SPM Model could be useful for class projects, or for basic level understanding of the voltage and flux density waveforms. The COMSOL model on the other hand, takes significant amount of processing power and time to generate the results, but the macroscopic

detail of the model is excellent. The reduced order model is supposed to generate all the results generated by the COMSOL model, with a lesser complexity, but it shows limitations with the electrolyte potential prediction.

Furthermore, from the current results of concentration profile, the state space model is not able to capture the dynamics at the localized location like the COMSOL model. Moreover, there is a limitation for which the state space model can work. For example, the total iterations of the system cannot be smaller than the order of the predicted system.

Also, as reported before, increasing the eigenvalues in the Reduced Order Model results in a significant increase in the simulation time, for an increase in eigenvalue number for 4 to 12, the simulation time increases 37 secs from the initial selection of 11 eigenvalues. It would be a good practice to find the tradeoff between the simulation time lost and the accuracy lost in the model.

The next chapter presents the development of a more elaborate set of PDE equations that incorporate aging mechanisms for the lithium-ion batteries. Then a continuum model will be developed to generate some results known for Li-ion batteries.

3 A novel integrated model

This thesis generates a new integrated porous electrode model of a lithium-ion battery that models various mechanisms of its degradation that have been found in the current literature. Contrary to the existing approach of modeling different aging behaviors at different scales, like particle, electrode, and cell level, this work brings all the degradation behaviors together in an integrated porous electrode theory, favoring a top-down modeling approach. Even if the increase in the computational complexity may seem large, there are optimization methods which could be employed to bring down the complexity to be used in an automotive battery management system.

The degradation mechanisms covered in the thesis include Solid-Electrolyte Layer growth, Li-plating, electrolyte dissolution, active area loss with cycling, capacity loss with calendar aging, mechanical deformation, and automotive vibrations. The equations are substituted to make a generalized PDE model that could be extended to pseudo 3D or 4D dimensions. COMSOL environment has then been utilized to draw correlations to experimental data.

3.1 Literature Review

There are many methods in the current literature that try to model the complexity of a lithium ion battery. The two objectives of such models are: first to replicate the intrinsic behavior of the charge and discharge, and second to find the reasons behind the battery degradation. These models can be classified into phenomenological and predictive. The later depends on recorded data to use techniques like neural networks to predict the behavior of the system. However, the former tries to use mathematical equations to model underlying processes to replicate the empirical results.

The phenomenological approach was first introduced by Doyle et al [27], based on Newman's porous electrode theory [19], that used a set of partial differential equations to model the movement of ions and particles in a battery. Since 1993, there have been significant developments in the model, and the modified porous electrode theory with heat generation as shown by Northman et al [29] has been used as the base model for integrating other degradation mechanisms suggested by other authors.

The first approach to modeling degradation was in the form of the solid electrolyte layer [SEI] presented by Safari et al [34] in 2009, and has been accepted as the most popular way to model the growth of SEI layer in negative electrodes. Lithium plating during overcharge was proposed by Perkins et al [17], which used the overcharge current flux to quantify the amount of lithium plated on the negative electrodes. Dai et al [35] worked in the dissolution of active materials and solvents, to report that the solid diffusion constant is inversely related as the active materials concentration in the battery. Further, there are other work in the literature that model the number of the actives sites [36], and other authors are going towards the coupling of mechanical behavior with the electrochemical behaviors of a battery.

Even if these models are adequate, their results are far from the real-life empirical results of a battery as they consider a single phenomenon. There are attempts in the literature to couple various scales and mechanisms together, but there is dearth of models which couple electrochemical behavior with its degradation. This paper presents a novel battery model which stitches an elaborate porous electrode theory with known degradation mechanisms to theoretically increase the accuracy of predictions.

The upcoming section of the thesis consists of the equations of the base model, and a review of the literatures that model specific degradation mechanisms. These mechanisms are stitched together to the base model in the following section 3. The section 4 of the thesis discusses the construction of a COMSOL model based on the equations and its results.

3.2 Equations: The modified Porous electrode theory

Equations in Table 1 represent the modified version of the porous electrode theory model. The partial differential equations can be extended to all 3 dimensions by increasing the number of variables, however for the simulations in this thesis, only two dimensions have been considered. This allows the model to be called a Pseudo 3D model, as the radius of the electrode particles (assuming them to be perfect spheres) is a pseudo dimension. The boundary conditions for the model can be seen in Figure 3-1, as shown by Northrop et al [29] .

Conservation of charge	Solid phase: $\nabla.\left(\sigma_s^{eff}\,\nabla\varphi_s\right) = a_s j_s$	Electrolyte phase: $-\nabla\cdot\left[\sigma_e^{eff}\,\nabla\phi_s\right] - \nabla\cdot\left[\kappa_e^{eff}\,\nabla\phi_e\right] + \nabla.\left[\frac{2\kappa_e^{eff}RT}{F}(1-t_+)\nabla\ln c_e\right] = 0$
Conservation of Mass	Solid phase: $\frac{\partial(\varepsilon_s c_s)}{\partial t} = \frac{1}{r^2}\frac{\partial}{\partial r}\left(D_s{}^{eff} r^2 \frac{\partial c_s}{\partial r}\right)$	Electrolyte phase $\frac{\partial(\varepsilon_e c_e)}{\partial t} = \nabla\cdot\left(D_e{}^{eff}\nabla c_e\right) + \frac{a_s(1-t_+^0)j}{F}$
Kinetics	Electrochemical Reaction Rate: $j = k_e(c_e)^{\alpha_a}\left(c_s^{max} - c_{s,e}\right)^{\alpha_a}\left(c_{s,e}\right)^{\alpha_c}\left\{\exp\left[\frac{\alpha_a F}{RT}\left(\eta - \frac{R_{film}}{\alpha_s}j\right)\right] - \exp\left[\frac{\alpha_c F}{RT}\left(\eta - \frac{R_{film}}{\alpha_s}j\right)\right]\right\}$ Overpotential: $\eta = \phi_s - \phi_e - U$	

Table 2 **:** Equations for the modified porous electrode theory (PDEs).

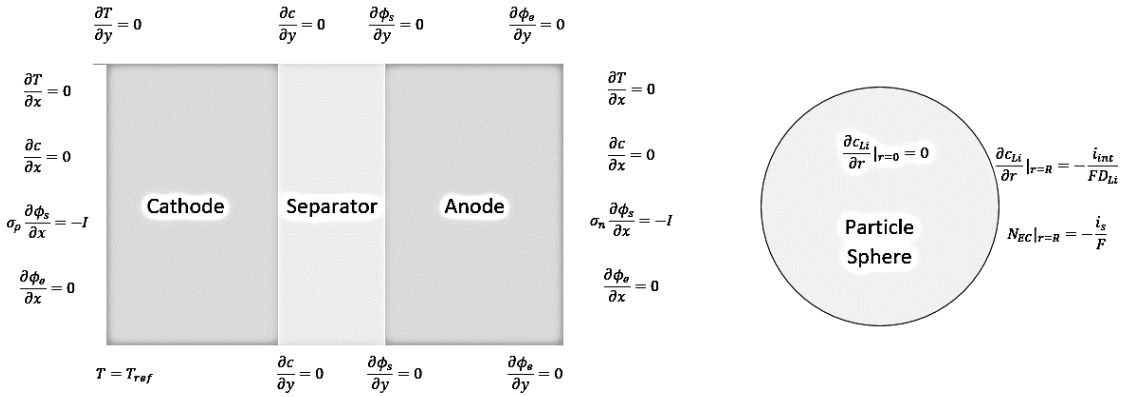

Figure 3-1: Boundary conditions of the modified porous electrode theory

3.3 Degradation Mechanisms

The scientific community agrees on multiple aging mechanisms which contribute to the capacity and performance degradation of a Lithium-ion battery. Smith et al [37] made a good tabulation of the known mechanisms, Table 3 lists the mechanisms covered in this work.

Mechanical	• Mechanical Stress and deformation • Automotive vibrations
Chemical	• Lithium plating during Overcharge
Electrochemical	• Side reactions • Solvent dissolution • SEI growth
Electro-chemo-mechanical	• Active site area loss due to cycling
Thermal Coupling	• Reaction rates increasing with higher temperatures

Table 3: Degradation mechanisms of LIB [38]

3.3.1 SEI growth

Solid electrolyte layer is understood to be the primary cause [36] of a Li-ion aging. According to Wertheim et al [39], the process starts when the voltage of graphite electrode drops below a certain threshold (typically 1.0V) with respect to the cathode. The initial formation of the SEI, during the activation procedure decides on the cycling performance for the rest of the life.

In the existing literatures, there are multiple proposed methods of reaching at the final product as the SEI, however, any of the processes with their current density could be used to predict the rate of the growth [34]. The rate of SEI growth, where δ is the length of the SEI (generally in nm) can be given by:

$$v = \frac{d\delta}{dt} = -\frac{i_s}{2F}\frac{M_{SEI}}{\rho_{SEI}} \mid (r = R + \delta) \qquad \text{Equation 23}$$

Here, $M_{SEI}$is the molecular weight, ρ_{SEI} the density of the SEI film, and i_s is the kinetic current density of the side reaction given by

$$i_s = -Fk_{f,s}c_{EC}\, exp\left[-\frac{\beta_s F}{RT}(\phi_s - \frac{\delta}{k_{SEI}} i_t)\right] \qquad \text{Equation 24}$$

The total current density i_t at the negative electrode can be given by

$$i_t = i_{int} + i_s \qquad \text{Equation 25}$$

Now it depends recursively to i_{int} ,the intercalation current density depending upon the butler-Volmer Kinetics, modified from the porous electrode model:

$$i_{int} = F\, k_{int}(c_e)^{\alpha_a}\left(c_s^{max} - c_{s,e}\right)^{\alpha_\alpha}\left(c_{s,e}\right)^{\alpha_c}\left\{\exp\left[\frac{\alpha_\alpha F}{RT}\left(\eta - \frac{\delta}{k_{SEI}} i_t\right)\right] - \exp\left[\frac{\alpha_c F}{RT}\left(\eta - \frac{\delta}{k_{SEI}} i_t\right)\right]\right\} \qquad \text{Equation 26}$$

The c_x are concentration of ions in electrolytes and electrodes, η is the overpotential, and k_{SEI} is the conductivity of the SEI layer. The material loss of the solvent can be given by [34], where ε is the concentration of active materials in the electrolyte.

$$\frac{\partial \varepsilon}{\partial t} = D_{EC}\frac{\partial^2 \varepsilon}{\partial r^2} - v\frac{\partial \varepsilon}{\partial r} \qquad \text{Equation 27}$$

3.3.2 Lithium Plating

The lithium plating behavior can happen in two major conditions of a battery operation: overcharging or a low temperature operation. It has also been argued that a high discharge rate results in the metal plating [36]. The work shown here tries to model the overcharge and the capacity fade and resistance increase associated with plating.

The method proposed by Perkins et al [17] is to modify the film resistance accounting for the new film due to the metal plating. The following equations represent the side reaction current density, or the rate of li-plating:

$$j_{plating} = min\left[0, k_n(c_e)^{\alpha_a}\left(c_s^{max} - c_{s,e}\right)^{\alpha_\alpha}\left(c_{s,e}\right)^{\alpha_c}\left\{\exp\left[\frac{\alpha_\alpha F}{RT}\left(\eta - \frac{\delta_{film}}{k_{Li}} i_t\right)\right] - \exp\left[\frac{\alpha_c F}{RT}\left(\eta - \frac{\delta_{film}}{k_{Li}} i_t\right)\right]\right\}\right] \qquad \text{Equation 28}$$

$$R_{film}(x,t) = R^0_{SEI}(x,t) + R_{Li}(x,t) \qquad \text{Equation 29}$$

Observe that the variables $k_{Li}$is the only variable localized to the Li plating process, and the length of the film δ_{film} included the SEI layer growth δ, and hence could potentially be used

to improve the SEI growth equation. This is the approach which would be followed in the next section of thesis to stitch various models together.

The capacity loss due to these two processes will be accounted for later.

3.3.3 Electrolyte/ active material Dissolution

The electrolyte dissolution is yet another phenomenon representing the active material loss. The simplest way to account for this method is find the rate of reaction which causes the dissolution. This will rate the change of active material ε with the following equation, as given by [35][36].

$$\frac{\partial \varepsilon}{\partial t} = -a_{c,i}\bar{V}r_{diss} \qquad \text{Equation 30}$$

Here, the *V* is the molar volume of the electrolyte or active material (like LMO in Li-Manganese-oxide cell), and r_{diss} is the dissolution constant for that species. Finally, this loss in the active material can be related to the original model by changing the diffusion coefficient and a side current density for dissolution:

$$D_s = D_s{}^0[1 - \left(\frac{\varepsilon^0 - \varepsilon}{\varepsilon^0}\right)^n] \qquad \text{Equation 31}$$

$$j_{sol}^{tilde} \sim -D_i^{eff}\nabla c_i \qquad \text{Equation 32}$$

3.3.4 Active site area loss

The active sites available for the transaction of ions change by two contradictory mechanisms: Fracture of particles, which increases the area, and isolation of particles which decreases the area. The current state of active sites is given by [36]:

$$a_c = a_i + a_f - a_{isolated} \qquad \text{Equation 33}$$

where $a_i$is the initial surface area given by $\frac{3\varepsilon_s}{r}$ [14] assuming the electrode is a collection of spheres on uniform radius. a_f and $a_{isolated}$ are the resultant area due to fracture and isolation.

$$\frac{d\left(\frac{a_f}{a_i}\right)}{dN} = k_f \qquad \text{Equation 34}$$

$$\frac{\mathrm{d}a_{isolated}}{dN} = k_{iso}a_i \qquad \text{Equation 35}$$

Here, N denotes the number of cycles. k_f are the material parameters which depends on the current, ΔSOC, SOC, temperature, and particle size [36]. This parameter is crucial to generate proper results for a high discharge behavior of a battery. k_{iso}, on the other hand, is an

evolution parameter for isolation. We see that these variables are highly empirical, and there are vast amounts of uncertain conditions which can lead model to an inaccurate result.

This equation would be coupled in the original model by altering the active site area variable in the flux equations as reduced by Narayan Rao et al [7].

3.3.5 Number of Cycles

When a battery is bought from a manufacturer, it has a listed number of cycles noted as the total life of the cell but a certain amount of degradation. However, this aging tests for cycling are conducted linearly for a specific SOC range and generally at 1C discharge rate. However, the effective cycle number of the cell might differ according to the behavior of the user. A weighted number of cycles could give a proper health estimation of a battery.

In this model, however, the number of cycles parameter is only used for estimating the surface area change, and the empirical tests to estimate k_f and k_{iso}must have a definitively measure to calculate the number of cycles. Hence, a rather simplistic approach of current integration is presented, as proposed by Alan [23]. Moreover, the weighted method of cycle estimation is an empirical aging data condensed into a single equation.

$$N = \int_{time} \frac{abs(I(t))dt}{Q_{cell}*2} \qquad \text{Equation 36}$$

The 2 factor comes in because it considers both charging and discharging of the cell, just for ease of modeling. Notice that, $Q_{cell}$is the initial capacity of the cell, not the updated degrading capacity.

3.3.6 Mechanical Deformation and stress

The mechanical deformation and stress could be divided into two segments: external and internal. The effect of external stresses like impact, pressure and tension have been found difficult to couple with electrochemical behavior. Moreover, the cylindrical cells do not tend to have external stress due to their packaging form. In this thesis, the internal volumetric stress has been modeled as shown by Xu et al [40].

The pure volumetric stress generated by lithiation is given by

$$\mu = \mu^0 + kTlog(\gamma x) - \Omega\sigma_m \qquad \text{Equation 37}$$

Here, σ_m is the mean stress, μ is the chemical potential of Li, and the $kTlog(\gamma x)$ represents the change in elastic energy under stress, and Ω is the partial molar volume of lithium in the electrode. In the mentioned work, the stress generated due to the Li_xSi particle has been modeled. The values of the stress would depend upon the number of intercalated ions, increasing the stress potential as intercalation increases.

This mean stress coupled with the partial molar volume can be incorporated in the current flux density equation of the original model:

$$i = i_o \left\{ \exp\left[\frac{\alpha_\alpha F(E-E_o)-\Omega\sigma_m}{RT}\right] - \exp\left[\frac{\alpha_c F(E-E_o)-\Omega\sigma_m}{RT}\right] \right\} \quad \text{Equation 38}$$

3.3.7 Automotive vibrations

According to the literature [41], the pouch cells do not experience any degradation with the vibrations. However, the cylindrical cells while going through a z-vibration tend to get loose mandrels which cause an increase in resistance or an apparent capacity loss. James et al [42] quantified the resistance increase by conducting experiments on a sample of 12 Lithium Nickel Cobalt Aluminum (NCA) batteries, subjecting them to 150 hours of vibration in 6 degrees of freedom. Using ANOVA analysis, they predicted with a 95% confidence level that the mean DC resistance was 2.45% at the end of the test. However, it was also reported in the paper that the cells excited to 6 degrees of freedoms experienced a slower rate of degradation as compared to cells which were left in static condition.

In another work by Fu et al [43], the change in resistance of the electrical connections in hybrid vehicle was quantified as a function of displacement frequency and the amplitude of the displacement, as given by equation 57.

$$\Delta R_{vibration} = k_{cyl,vib} \Delta D f^2 \quad \text{Equation 39}$$

Even though some works [44] do report that the vibrations destroy the SEI layer formed during initial cycling to replace it with film with electrolyte decomposition, we don't have quantified results for the same. Further, it has been recognized repeatedly recognized [42] that there is no degradation at the electrochemical level with vibrations.

Hence, this equation could be used to predict the resistance increase in a cylindrical cell. The constant $k_{cyl,vib}$ can be found out with experimental results. As reported in [43], the value of the constant should have a quadratic relationship peaking at mid-range frequencies.

This equation will be incorporated in the final model through the increase in the cell resistance.

3.3.8 Heat generation

The heat equations integrated in this work are the ones proposed by Newman and Pals [45], which complements the porous electrode theory. It summarizes 3 types of heat generated in a battery: reversible heat generation (Q_{rev}), Active polarization heat (Q_{rxn}) which is generated because of disturbing the OCV equilibrium, and ohmic heat (Q_{ohm}). The latter is composed of

three components, the heat because of Li-intercalation, second the li-ion transformation, and finally the resistance due to current collectors [28]. Because the thickness of the current collectors is limited to few micro-meters [46], the current collector heat is not of a great significance.

Finally, the heat interaction of a li-ion batteries can be related to the boundary conditions of energy conversation through the Newton's law of cooling [28] as given by following equation. Here, ε_t is the blackness of Li-ion surface, T_{amb} is the ambient temperature of the pack, *h* is the heat change coefficient, σ is the Stefen-Boltmann constant, and λ is the flux density.

$$-\lambda \nabla T = -h(T_{amb} - T) - \varepsilon_t \sigma\left(T_{amb}^4 - T^4\right)$$

3.4 Substitution and Model generation

As described in the previous section, all the mechanisms are tied together by interconnected variables to generate the model shown in Table 4. The process of explaining each variable can be observed by referring to the previous chapters. There is an apparent increase in the complexity of the model in case of algebraic and differential equations, however the number of partial differential equation remains constant.

The resistance of this film is the major cause of the performance degradation of a li-ion battery. The total length of the film, as discussed before can be given as

$$\delta_{\text{film}} = \delta_{\text{o}} + \delta_{Li\ plating} + \delta_{SEI} + (R_{vibration}) * k_{SEI} \quad \text{Equation 40}$$

The overall capacity loss in the model due to shown mechanisms can be given by:

$$\frac{\partial Q(t)_{usage}}{\partial t} = max\left[A \int_0^l j_{plating}(x,t)\,\mathrm{d}x\,, a_{c,i}\bar{V} r_{diss}\right] + A \int_0^l j_{sei}(x,t)\,\mathrm{d}x \quad \text{Equation 41}$$

Here, *l* is the length of the cell, *A* is the total surface area of the electrode. It can be observed that in this thesis, for the capacity loss calculation, the homogeneity in the y direction has been considered.

However, there is another type of aging which has not been modeled in the dynamic porous electrode theory so far. Calendar aging, or shelf aging of lithium ion batteries can be quantified with two major factors: state of charge of storage, and the temperature of the storage conditions. In basic models, this is exhibited as increase in the DC impedance, with a reversible and irreversible component. However, the primary mode of calendar degradation is the loss of cyclable Lithium [47] and in very extreme situations (high temperature and SOC), there is a loss of active materials.

Further, in a work by Dong Jiang[48], there has been a mathematical relation developed which can distinguish between the calendar and cyclic aging. The SEI formation during storage can be given by:

$$i_{storage} = -Fk_{f,storage}c_{EC}\, exp\left[-\frac{\beta_s F}{RT}\left(\phi_s - \frac{(\delta_{film}+\delta_{calendar})}{k_{SEI}} i_{storage}\right)\right] \quad \text{Equation 42}$$

$$\frac{d\delta_{calendar}}{dt} = -\frac{i_{storage}}{2F}\frac{M_{SEI}}{\rho_{SEI}} \quad \text{Equation 43}$$

Here, $k_{f,storage}$ is the rate of side reactions during calendar aging which would be dependent on the State of Charge and the temperature conditions of the storage. There is no side current density during an idle battery behavior, hence the complexity of the calculation is reduced. Hence, the overall calendar aging of a cell can be given by

$$\frac{\partial Q(t)_{calendar}}{\partial t} = \int_0^l i_{storage}\, \mathrm{d}x \quad \text{Equation 44}$$

It can be observed by this equation that both the reversible and irreversible calendar capacity losses can be modeled by the same equation, keeping in account that the reaction rate constants would be different for the two different mechanisms.

3.5 Summary and limitations

The presented work provided a framework to add multiple mechanisms through an integrated model. This model could be extended even further by defining the variables like conductivity and diffusivity to vary as a function of distance of local SOC. In contrast, work on reducing this model could help bring all aging mechanisms on a single page on an inexpensive BMS.

Even if the electrochemical model simulates the behavior of an actual battery, there remains variables for the behaviors which need to be evaluated using empirical data. Obtaining empirical data can be difficult in most of the situations as they are not reported by the manufacturer, and some variables like the kinetic rate constant have no definite way of being measured, this limits the effectiveness of the model. Other variables like the diffusion coefficient for the solid electrodes measured in the laboratory with an open cell may not be able to capture the dynamics of a closed cylindrical cell that is undergoing pressure of cycling under the arrangement in a pack.

Further, there are many aging mechanisms that still need to be incorporated in the model: the SEI decomposition, electrolyte oxidation, manufacturing defects are to name a few. The former two can be incorporated by adjusting the coefficients for the SEI growth rate, and electrolyte dissolution. Similarly, the model assumes the fracture and isolation evolution parameters as constant, however, their dependency on the ΔSOC and other parameters like temperature would be very crucial. Hence, this model could incorporate the mechanisms that have not been covered in the thesis by means of adjusting the coefficients of the equations. Also, the equations used for transport of a singular species, must be replicated for simulating the flux of the transport of minor species, such as byproducts and stabilizers for the electrolyte.

Table 4: Equations for the coupled porous electrode theory. [27], [49]

Active Surface Area change	*Positive electrode:* $a_{c,p} = a_{i,p} + a_i k_{f,p} N - k_{iso,p} a_i N$		*Negative electrode:* $a_{c,n} = a_{i,n} + a_i k_{f,n} N - k_{iso,n} a_i N$
Solvent Dissolution	$\frac{\partial \varepsilon}{\partial t} = -a_{c,i} \bar{V} r_{diss}$		$D_{s,i} = D_{s,i}{}^0 [1 - \left(\frac{\varepsilon^0 - \varepsilon}{\varepsilon^0}\right)^n]$
Conservation of charge	*Solid phase:* $\nabla . \left(\sigma_s^{eff} \nabla \varphi_s\right) = a_{c,i} j_t$		*Electrolyte phase* $-\nabla \cdot \left[\sigma_e^{eff} \nabla \phi_s\right] - \nabla \cdot \left[\kappa_e^{eff} \nabla \phi_e\right] + \nabla . \left[\frac{2\kappa_e^{eff} RT}{F} (1 - t_+) \nabla \ln c_e \nabla \phi_e\right] = 0$
Conservation of Lithium	*Solid phase:* $\frac{\partial(\varepsilon_s c_s)}{\partial t} = \frac{1}{r^2} \frac{\partial}{\partial r} \left(D_{s,i}{}^{eff} r^2 \frac{\partial c_s}{\partial r}\right)$		*Electrolyte phase* $\frac{\partial(\varepsilon_e c_e)}{\partial t} = \nabla \cdot \left(D_e{}^{eff} \nabla c_e\right) + \frac{a_s (1 - t_+^0) j_t}{F}$
SEI Current density	*Modified Current Density at electrodes* $j_t = j_{int} + j_{sei}$		$j_{sei} = k_{side} (\varepsilon)^{\alpha_a} \exp\left[\frac{\beta_s F}{RT} \left(\phi_s - \frac{\delta_{eqv,film}}{k_{SEI} * \alpha_{n,c}} j_t - \Omega \sigma_m\right)\right]$
Kinetics with overcharging and mechanical stress	*Electrochemical Reaction Rate* $j_{int} = k_e (c_e)^{\alpha_a} \left(c_s^{max} - c_{s,e}\right)^{\alpha_\alpha} \left(c_{s,e}\right)^{\alpha_c}$ $\left\{\exp\left[\frac{\alpha_\alpha F}{RT} \left(\eta - \frac{\delta_{eqv,film}}{k_{SEI} * a_{c,p}} j_t - \Omega \sigma_m\right)\right] - \exp\left[\frac{\alpha_c F}{RT} \left(\eta - \frac{\delta_{eqv,film}}{k_{SEI} * a_{c,n}} j_t - \Omega \sigma_m\right)\right]\right\} - j_{minor}^{tilde}$		*Overpotential* $\eta = \phi_s - \phi_e - U - \frac{j_{plating}}{\alpha_c}$ $j_{plating} = \min\left[0, k_n (c_e)^{\alpha_a} \left(c_s^{max} - c_{s,e}\right)^{\alpha_\alpha} \left(c_{s,e}\right)^{\alpha_c} \left\{\exp\left[\frac{\alpha_\alpha F}{RT} \left(\eta - \frac{\delta_{eqv,film}}{k_{Li}} i_t\right)\right] - \exp\left[\frac{\alpha_c F}{RT} \left(\eta - \frac{\delta_{eqv,film}}{k_{Li}} i_t\right)\right]\right\}\right]$
Temperature extrapolations	$U_i(T_i, \theta_i) = U_{i,ref}(T_{ref}, \theta_i) + (T_i - Tr) \left[\frac{\partial U_i}{\partial T}\right]\Big\vert_{Tref}$	$D_{s,i}{}^{eff} = D_{s,i} \exp(-\frac{E_a^{D_i}}{R} \left[\frac{1}{T} - \frac{1}{T_{ref}}\right])$, $i = p, n$	$\kappa_i{}^{eff} = \kappa_i \exp(-\frac{E_a^{\kappa_i}}{R} \left[\frac{1}{T} - \frac{1}{T_{ref}}\right])$, $i = p, n$
Heat	$\rho_i C_{p,i} \frac{dT_p}{dt} = \nabla \cdot \lambda_i \nabla T + Q$ *(Internal energy conservation equation)*		
	Solid Phase $Q = Q_{rxn,i} + Q_{rev,i} + Q_{ohm,i} + Q_{ohm,e}$, $i = p, n$, *c= collector*		
	$Q_{rxn,i} = Fa_i j_{int,i} (\phi_s - \phi_e - U_i)$, $Q_{rev,i} = Fa_{c,i} j_{int,i} T_i \frac{\partial U_i}{\partial T}$, $Q_{ohm,i} = \left[\sigma_{s,i}^{eff} \left[\nabla \phi_{s,i}\right]^2\right] + \left[\kappa_i^{eff} \left[\nabla \phi_{e,i}\right]^2\right] + \left[\frac{2\kappa_i^{eff} RT}{F} (1 - t_+{}^0) \nabla \ln c_e \nabla \phi_{e,i}\right] + \sigma_{c,i}^{eff} \left[\nabla \phi_{c,i}\right]^2$		
	Electrolyte Phase $Q = Q_{ohm,e} = \left[\kappa_{2,e}^{eff} \left[\nabla \phi_e\right]^2\right] + \left[\frac{2\kappa_{2,e}^{eff} RT_e}{F} (1 - t_+{}^0) \nabla \ln c_e \nabla \phi_e\right]$		
Capacity	$\frac{\partial Q(t)_{usage}}{\partial t} = max\left[A \int_0^l j_{plating}(x,t)\, dx, a_{c,i} \bar{V} r_{diss}\right] + A \int_0^l j_{sei}(x,t)\, dx$, $\frac{\partial Q(t)_{calendar}}{\partial t} = \int_0^l i_{storage}\, dx$		

The heat model presented in this work ties up the total heat generation with a single temperature state variation on the cell level, which ignores the uneven distribution through the cell. Lai et al. [28] reported that the region near tabs have lower temperature as compared to the rest of the cell because of better conductivity of collectors.

Further, this model built over the framework of the porous electrode theory did not address the limitations of the original theory itself. Based on volume averaged quantities, this model does not consider the in-homogeneities present in the length scales of the electrode [27]. Also, this model describes only the solid-solution active materials, but the electrodes used today, like LFP, reflect multiple stable phases of varying equilibrium concentrations which can't be described without empirical modifications [30].

Finally, the computational complexity of the current model would be too high for inexpensive computational purposes, and the assumptions could reduce the system of equations to make compromises on the actual prediction. Hence, work done by Northrop [50] [49], multi-domain modeling shown by Smith et al. [51] [30] could be further approached to reduce the model. We will discuss these works in upcoming chapters. The next chapter presents a summary of parameters inherent to the presented model, and the scope of the variables.

4 Model Parameters

The major challenge towards developing physical model is the estimation and assumption of the parameters used in the model. The sources for this information is the manufacturer [52], or the experimental data reported in the literature [4] [53]. Further, the accuracy of the reported variables can depend on measurement techniques and equipment, as well as manufacturing processes which could cause variations of the parameters [12] in products produced at different time lines.

With a goal to represent many battery chemistries, the parameters reported in this chapter are shown as a range of values. The first section presents an analysis of the parameters used in the work. The next section reports the parameters used in this work.

4.1 Parameter analysis

A predictive understanding of a LIB arises from two basic reasons [54]: non-linearity of the internal phenomena, and inhomogeneity in the internal structure. Even if the systems of equations presented by Doyle and Newman [27] present a strong case to model the behavior, they need a conjunction of non-linear parameters to complement them [55]–[57]. The following text visits these linear and non-linear dependencies to the other parameters and state variables of a battery.

4.1.1 Active interfacial surface area ($a_{c,i}$)

As discussed in Chapter 1, the porous electrodes are assumed to be made of uniform spheres, with the electrolyte flushing the gap between these spheres. The $a_{c,i}$ parameter, where i denotes subscripts for positive and negative electrode represents the solid area exposed to the liquid phase per unit volume, and can be given by following equation [14].

$$a_{c,i} = \frac{3\varepsilon_i}{r} \qquad \text{Equation 45}$$

The parameters ε_i and r are volume fractions of the electrodes and the particle radius, which would be discussed later. This thesis relates change in this surface area, as discussed in the section 3.3.4 , using the parameters of fracture and isolation coefficients. There parameters could be estimated by measuring a gradual change in the interfacial area, however, there are no significant literatures available on measuring the same. To use the above equation, tracer tests [58] could be conducted to calculate the absorption of the liquid in the porous materials, and the mean radius could be estimated through an electron microscopy. Also, there are products like Beckman Coulter SA3100 surface area analyzer [59], that could be used to estimate the surface area of the whole electrode using the absorption of gas molecules on solid surface.

The interfacial surface area has units of m^{-1} and varies in the order of 10^4 to 10^6 units. Further, this parameter can also be used to account for mechanical degradation caused by external parameters like stress, manufacturing defects.

4.1.2 Active material concentration (ε) and Rate of Dissolution (r_{diss})

Active materials in an electrode are the chemical compounds which interact with the cycling lithium ions in a LIB. Their loss is one of the primary causes of aging of LIB as it reduces the rate of transport of charge and mass in the electrode [36]. The quantification of the active material concentration with the molar volume of the electrolyte has been discussed in the section Electrolyte/ active material Dissolution 3.3.3.

Electrolyte in a LIB is typically composed of 3 components, a solvent, lithium salt, and some minor species such as additives added for electrolyte stability [58]. The minor species induce reactions interacting with both the electrodes which make the battery processes difficult to track. Assuming the concentration of the minor species to be diluted and that the flux of the mass exchange is negligible, this model quantifies only the loss of active materials to participate in aging. However, the flux term $j_{\text{minor}}^{\text{tilde}}$ could be used for averaged reduction of flux because of minor species.

For estimating the rate of dissolution, the first step is to understand the mechanisms that cause this phenomenon, which vary for different electrode materials [36]. For example, for Lithium Cobalt Oxide electrodes, it is understood in the scientific community that the delithiation starts with exchange of Li^+ ion with H^+ ions in the electrode lattice. Further, in the work by Billy at al. [59], a step by step procedure to estimate the dissolution rate is noted. The method involves the use of X-ray photoelectron spectrometry, X-ray diffraction, and transmission electron microscopy to understand the leaching process.

This method presents a limitation on the development of aging model for a conceptual battery chemistry, as the electrode material must be synthesized to find out the unintended dissolution phenomenon.

4.1.3 Solid phase diffusion coefficient ($D_{s,i}^{eff}$)

The solid phase diffusion is incorporated in the porous electrode theory through the Fick's law of diffusion as mentioned in chapter 2. This quantifies the rate of diffusion of lithium ions through the solid medium as a function of time and particle radium, r.

Having a rigorous approach to the coefficient increases the complexity of the model, and increases the computational cost of the model [33]. However, it is necessary to express the effective coefficient as a function of temperature and the active materials, as shown in the temperature extrapolations in Chapter 3, and the section 3.3.3.

In other literatures, this coefficient is reported as a function of the average Li-ion concentration in the electrode (signifying DOD) [22]. The typical values of the solid diffusion coefficients lie in the orders of 10^{-15} to 10^{-13}[38], however there is a variation of multiple orders of magnitude, showing that it is a poorly measured parameter [22] .

The methods employed to measure the solid phase diffusivity are intermittent titration and electrochemical spectroscopy (EIS, EVS) [60]. In the potentiostatic intermittent titration method, a series of 15 minutes of negative incremental potential pulses with 15 minutes relaxation time are applied through a whole discharge cycle, and the current development is related to the diffusion coefficient [61].

4.1.4 Liquid phase diffusion coefficient ($D_{e,i}^{eff}$)

The transfer of Li-ions in the liquid medium, both in the separator and suspended through the solid electrolyte and quantified by the liquid phase diffusion coefficient. Even if the coefficient generally varies by one order of magnitude from positive to negative electrode [62], the presented model in this work uses a constant value of this coefficient.

As the electrolytes are made up of additives, charged and uncharged carriers [36], and byproducts of the aging mechanisms, like dissolution, corrosion, electroplating [61], the estimation of this parameter is difficult. In literatures, this value has been reported to vary between orders of 10^{-9} to 10^{-11} [m2/s].

In-situ NMR (Nuclear Magnetic resonance) imaging is one of the popular methods to study electrolyte transport properties. By observing the salt concentration inside the cell in response to various current profiles can be used to predict variables like diffusivity, conductivity, and transference number[63]. Di-electric spectroscopy could also be used for predicting these variables as shown by Munar et al. [62]. The electrolyte medium with known dielectric constant is put between two electrodes, and the phase angle (θ) of the dielectric permittivity gives the diffusion coefficient by the following equation.

$$D_{e,i}^{measured} = \frac{2\Pi(frequency\ of\ EIS)^{max}(Length\ of\ the\ sample)^2}{32\cdot(tan\,\theta)^3_{max}} \qquad \text{Equation 46 [62]}$$

4.1.5 Solid Phase conductivity (σ_s^{eff})

The conductivity of the solid electrode is generally assumed to be dependent on the distribution of black carbon present in the lithium oxide electrodes, and as a function of the state of lithiation (DOD) [22]. Further, the Bruggeman's relation is used to effectively estimate the conductivity considering the tortuosity (τ), the active volume fraction (ε_s), and porosity (δ) [25] given by following equation.

$$\sigma_{eff} = \frac{\varepsilon_s \sigma \delta}{\tau} = \sigma {\varepsilon_s}^{brug}$$ Equation 47

The effective solid phase conductivity is always smaller than the measured conductivity, and the assumed value of the Bruggeman's exponent is assumed to 1.5. The typical value of effective solid phase conductivity lied in orders of 10^{-2} to 10^{2}[S/m].

The measurement of solid phase conductivity is done through a four-point probe technique [61], which is basically an electrical impedance measuring technique.

4.1.6 Liquid Phase conductivity (κ_e^{eff})

The conductivity of an electrolyte can be explained as the ability to conduct electricity. Similar to the solid phase conductivity, the effective liquid phase conductivity can also be expressed with the Bruggeman's exponent[25]. However, the values of the exponent are reported different for the separator and the electrodes, the conductivity being higher at the separator than the electrodes. [22]

The conductivity of solutions is generally reported at 1M, and lies between ranges of 1.2 to 1.8 [S/m] [22] at a temperature of 50°C. Further, at -40°C the conductivity drops to 10 times smaller [22].

The electrolyte conductivity could be measured using the methods reported before such as dielectric spectroscopy [62] and conductivity meter [64]. The variables causing complexity in the measurement of these variables have already been mentioned in the section 4.1.4.

4.1.7 Transference number (t^+, t^-)

Transference, or transport number represents the fraction of the solid lithium flux contributing to the change in electrolyte lithium concentration[25]. In other words, this number represents the fractional current carried in the electrolyte by lithium-ions.

Like the other transport parameters of a battery, the transference or transport number is also generally reported at 1M[22]. This value is generally reported to be equal to 0.37, with maximum and minimum range of 0.2 to 0.5 [22], however there is disagreement on if the transference number increases or decreases with an increase in the solvent concentration[65], [66].

The measurement of transport number is the more standardized: Hittorf and moving boundary method [22]. The former up depends on the coulomb comparison of the current flow and the species flow throw at an electrode, and the difference between the net increase of concentration and current can give the number. The moving boundary method, however, quantifies the number as the movement of the boundary between two interfaced electrolytes

in the influence of an electric field. There are more methods as suggested by Zugmann et al. [67] using electrostatic theory and NMR.

4.1.8 Kinetic Rate constant (k_o)

The rate constant of the reaction in a lithium-ion battery is one of the most important parameters to quantify the performance of a lithium-ion battery, but cannot be measured in a closed system like lithium-ion batteries [22]. It depends dynamically on the output required of the batteries, as quantified by the Butler-Volmer reaction. In other literatures, the reaction rate constant is generally estimated by the initial current density, that varies with temperature and concentration of lithium ions in each electrode [14].

A known way to estimate the change in reaction rate is via the Arrhenius relationship [25], where the activation energy (E_a) of reactions could be used to predict the rate of reaction, as shown in the following equation, where k_f^0 is a constant determined experimentally at reference conditions. A knowledge of undergoing multispecies interactions, the reaction rate could represent a balanced form for all reactions.

$$k = k_f^0 \, exp\left(\frac{E_a}{RT}\right) [25] \qquad \text{Equation 48}$$

The literatures report the reaction rate constant lies between orders of 10^{-14} to 10^{0} [22] [mol m-2 s-1] and it could be inferred that this parameter is poorly estimated in the existing literature.

4.1.9 Other variables

The open circuit potential (U_i) is reported for both the electrodes as a function of temperature and SOC. It is relatively easy to measure as compared to variables discussed prior to this section, using apparatuses such as rotating disk electrodes. A typical equation representing this state variable has been mentioned in Chapter 2.

The lithium concentrations in both electrodes ($c_{e,i}$) is generally specified by manufacturers, specifying the concentrations equivalent to 0 and 100% SOC. However, in battery modeling, there is an approach to separately define the two variables seemingly unrelated to each other through the Fick's law of diffusion at both electrodes. In the work done by Dey et al [68], they propose an estimation scheme where the concentration of positive electrode is estimated as a function of negative electrodes concentration.

The values of outer cell dimensions like thickness, length of electrodes is specified by the manufacturer and could vary according to the cell geometry. The particle radii, r reported in literatures varies from 10^{-10} to 10^{-9} [m] [22].

4.2 Tabulated parameters used in work

The selection of a battery chemistry for the model depends on two constraints: the availability of data in the current literature, and the known high discharge behavior of the chemistry. Due to the eclectic nature of equations that have been reported in the work, the data have been collected from variety of sources [10], [24], [56], [57],[55]. Hence, the final reported values represent a ballpark value of the parameters of a typical lithium-ion cell for providing an engineering reference. Empirical experimentation would be required to get the exact values of parameters.

Table 4 summarizes the data used for the model development, adding on to the model development by Gregory pelt [25].

4.3 Summary

In summary, there is seemingly a lot of disagreements amidst the data reported in the literature for the values of electrochemical and transport parameters. Developing a standardized methodology for measuring and calculating the parameters could help in better quantification the accuracy of the electrochemical models.

Most parameters are reported as constant, or just as the function of temperature, have the potential to be expressed as function of the lengths of the electrode, and some other state variables. This chapter could be used as a reference to revisit a specific parameter in question. The next chapter describes the development of the model in COMSOL and Mathematica environment.

Table 5: Nomenclature and parameters used in the model for the following chapter. The data has been collected from multiple references [22], [25], [40],[10], [57], [68],[14], [24] representing ballpark figures.

Sym	Description	Estimated value			Sym	Description	Estimated value		
$k_{f,s}$	Rate constant SEI [mol m-2 s-1]	1.36e-12 m/s 1.36e-7 (OCV storage)			$a_{i,initial}$	Active surface area [nAn]	Calculated by porosity and particle radius		
Ɛ	Solvent active material [mol/m3]	4541			D_{EC}	Diffusion rate in SEI equation [m2/s]	6.8e-21 m2/s, 3.7e-19 (OCV storage) [34]		
β_s	SEI Charge transfer coeff. [nAn]	0.5			r	Particle radius [µm]	12.5	8	
κ_e^{eff}	Liquid phase conductivity [S/m]	2*R*T/F*(1-t_+)			σ_m	Mean Stress ($\frac{\sigma_{kk}}{3}$) [Gpa]	10		
Kiso	Isolation evolution param {nAn]	N: 5.18 e-5	P: 1.07 e-8		Ω	Volume fraction of Li_xSi particles [V/GPa]	0.025		
Kf	Fracture evolution param [nAn]	N: 2.39 e-6	P: 2.87 e-7		ΔD	Amplitude of vibrations [mm]	0.4		
R	Gas constant [J mol-1 K-1]	8.314			$k_{cyl,vib}$	Vibrations coefficient [nAn]	7.2e-4		
r_{diss}	Rate of dissolution [mol/(m2s)]	Neg: 0	Pos: 8e-10		f	Frequency of vibrations [Hz]	100 Hz		
brug	Bruggeman's exponent [nAn]	1.5			k_e	Normalized Reaction rate constant [mol m-2 s-1]	Neg: $1.2 \times 10^{-5} \exp\left(\frac{-20000}{R}\left(\frac{1}{T}-\frac{1}{298.15}\right)\right)$		
n	Empirical factor diffusivity [nAn]	0.12					Pos: $3.7 \times 10^{-6} \exp(-\mathrm{SOCp})\exp\left(\frac{-30000}{R}\left(\frac{1}{T}-\frac{1}{298.15}\right)\right)$		
α_a	Charge transfer coefficient [nAn]	0.5			D_e^{eff}	Electrolyte Diffusion Coefficient [$m2\ s-1$]	$7.51e-4 \times 10^{-4.43\left(\left(\frac{54}{T-229-0.05ce}\right)2.2\times10^{-4}Ce\right)}$		
K_{SEI}	Conductivity of SEI layer [S/m]	5e-6			D_s^{eff}	Solid Diffusion Coefficient [$m2\ s-1$]	Neg: $3.9 \times 10^{-14} \exp\left(\frac{-35000}{R}\left(\frac{1}{T}-\frac{1}{298.15}\right)\right)$		
M_{SEI}	Molecular mass of SEI [kg/mol]	0.162					Pos: $\frac{1.18\times10^{-18}}{(1+SOCp)^{1.6}} \exp\left(\frac{-35000}{R}\left(\frac{1}{T}-\frac{1}{298.15}\right)\right)$		
ρ_{SEI}	Density of SEI [kg/m3]	1690			σ_i^{eff}	Solid phase conductivity [S m-1]	100	3.8	
δ^0	Initial length of the SEI layer [nm]	5			t_+	Transference number [nAn]	0.363		
$\bar{V}$	Solvent Molar Vol [m3 mol-1]	4.1389e-5			$\varepsilon_{e,i}$	Volume fraction of the electrolyte [nAn]	Neg: 0.33	Sep: 0.54	Pos: 0.332
$E_a^{D_i}$	Activation energy [kJ/mol]	18	4		$c_{s,\max}$	Max solid concentration of Li [mol m-3]	Neg: 10352	Pos: 7524	
λ	Thermal conductivity [W/m K]	1.3	0.099	1.04	L	Thickness of the battery (µm)	100	52	183
C_p	Specific heat of the cell [J/kg K]	1240	1518	1437	ρ	Density of the cell [kg m-3]	4740	1210	5031
Subscripts: i for p,n: p- positive electrode, n- negative electrode, the three columns in a section represent negative electrode ,sep, and positive electrode respectively [nAn] - dimensionless									

5 Simulation and Results

There are two approaches towards development of battery models: increasing the complexity of the models to capture more physical processes or reducing the complexity of the models to make them suitable for real time applications.

This thesis, so far, has addressed the need to increase the complexity of the model, and this chapter targets how to generate results to simulate to the model. Running this computationally expensive model brings with it a need of mathematical reduction, an aspect that is not in the scope of this thesis. However, the first section presents a literature review of a few mathematical methods before moving to model generation.

5.1 Literature review

Conventionally, the PDEs have always been used to model real life scenarios. There have been numerical methods to solve them equations like finite element method, finite difference, Galerkin approximation etc. Most of the methods have been successfully implemented in current generation computational software like MATLAB and Maple, but these methods struggle with high computational requirements, which is not suitable for mobile applications of lithium-ion batteries [29].

Northrop et al [29], [49], [50], [69] have contributed significantly towards the model reformulation of the physical models of lithium ion batteries, using methods like coordinate transformation and orthogonal collocation.

Beginning with simple transformation [32], the pseudo 2D dimension of the solid diffusion in the electrolyte is removed by polynomial profile approximation, where the solid concentration is represented as a function of particle surface concentration. In co-ordinate transformation [49], the three region cell is converted into a single region by normalized co-ordinates. This reduces the complexity of the equation as all variables can be expressed as a function of single variable x. The method of orthogonal collocation [49] estimates a variable of interest by a summation of linearly independent trial functions, as shown in the following equation. The weights to the approximated functions are found by minimize the residuals while keeping the computational complexity.

$$c_p(x,t) = A_p, c(t)x^2 + \sum_{k=0}^{N_P} B_{p,c,k}(t)\cos(k\pi x) \qquad \text{Equation 49}$$

Model order reduction techniques by approximating frequency response through Padé approximation and residue grouping methods are the most popular methods taken in current scientific community [70]. Introduced by mathematician Henri Padé, this method suggests estimating a function through power series of the same order. It is a special time of estimator that has both numerator and denominator coefficients in the approximator functions.

Further, the implementation of reduced physical models is explored in some literatures [29], [71]. It is explored that some parameters like electrolyte concentration and overpotential that could have detailed equations to capture high charging and discharging behavior.

In summary, there has been a lot of work to reduce the models mathematically for automotive BMS applications, and a selective approach can be taken tailored to the performance required for the condition. This thesis, however, focusses on the generating simulations of the model in software environment, and does not address the mathematical reduction techniques.

5.2 Model Development

There are mathematical tools which allow using these mathematical methods to be called upon for solving the set of differential equations. There was plethora of options to choose from: MATLAB, COMSOL, Mathematica are one of the most popular ones to choose. This thesis started with using Mathematica as the first approaches because of their rather intuitive mathematical modeling, and easy post processing of the data. However, we can see that the capabilities of the software are limited, especially for solving time delayed PDE's. Using COMSOL was also explored but getting around circular dependency of the current density is a difficult problem.

This thesis uses high computational power and software tools rather than solving the equations by reduction methods as described in the last section. The upcoming text summarizes the development of the model, and snapshots to regenerate the results.

5.2.1 Mathematica 12 Prerelease

Mathematica, originally, was marketed towards physicists and mathematicians for the nature of mathematical manipulation of this software surpasses any of the other packages available currently. However, they have been expanding their domain to address more real-life simulations and engineering problems. The perks of using this software is that the same package could be used for developing mathematical tools of reduction, taking heuristic approach to solving the model, import real time data, and many others. In the next chapter of this thesis, the feasibility of teaching neural networks to estimate the solutions of the PDE's in this environment is talked about.

The stages of development of the model is to initialize variables, set the boundary conditions in the specified domain, and specify the initial conditions, and call a solver by selecting a method of estimation. The Figure 5-1 captures a snapshot of the developed model.

The model was not used to generate results because of an apparent incapability of the model to solved delayed PDE's, and circular referencing that is inherent in the physical model at the current density equations and the growth of the SEI. Also, the inbuilt methods of lines, and

stiffness switching methods do not work well with parabolic PDE's. The software package of PDE's was only introduced in Mathematica in the year 2014, and there is a long way to go for the software to match Multiphysics software like COMSOL for solving domain based PDE's.

```
In[ ]:= solveFor = {δeqvfilm[x, r, t], csp[x, r, t], csn[x, r, t], ce[x, r, t], cEC[x, r, t], ϵe[x, r, t],
        ϕs[x, r, t], ϕe[x, r, t], SOCn[t], SOCp[t]};

In[ ]:= {eqns = {
        D[ϵsp * csp[x, r, t], t] == D[Dspeff * (r^2) * D[csp[x, r, t], r], r] / (r^2),
        D[ϵsn * csn[x, r, t], t] == D[Dsneff * (r^2) * D[csn[x, r, t], r], r] / (r^2),
        D[ϵe[x, r, t] * ce[x, r, t], t] == D[(Deeff * D[ce[x, r, t], {x}]), {x}] + (acp * (1 - tplus) * js[x, r, t] / F),
        D[σseffn * D[ϕs[x, r, t], {x}], {x}] == acn * js[x, r, t],
        D[σseffp * D[ϕs[x, r, t], {x}], {x}] == acp * js[x, r, t],
        -D[σseffn * D[ϕs[x, r, t], {x}] , {x}] - D[κeeff * D[ϕe[x, r, t], {x}] , {x}] +
          D[(2 * κeeff * R * T / F) * (1 - tplus) * D[ce[x, r, t], {x}], {x}] == 0,
        D[δeqvfilm[x, r, t], t] == -js[x, r, t] * Msei / (2 F psei),
        D[cEC[x, r, t], r] == DEC D[cEC[x, r, t], {r, 2}] - D[δeqvfilm[x, r, t], t] * D[cEC[x, r, t], r],
        jint[x, y, t] == (ken * (ce[x, r, t]^αa) * ((csmaxn - csn[x, r, t])^αa) * (csn[x, r, t]^αc)) *
          (Exp[((αa F / (R T)) * (η[x, r, t] - (δeqvfilm[x, r, t] * js[x, r, t] / (kSEI * acp)) - Ω σm))] -
            (Exp[(αc F / (R T)) * (η[x, r, t] - (*δeqvfilm[x,r,t]*js[x,r,t]/(kSEI*acn)*)Ω σm)])),
        js[x, r, t] == (ken * (ce[x, r, t]^αa) * ((csmaxn - csn[x, r, t])^αa) * (cEC[x, r, t]^αa)) *
          (Exp[(βs F / R T) * (ϕs[x, r, t] - (*δeqvfilm[x,r,t]*js[x,r,t]/(kSEI*acn)*)Ω σm)]),
        η[x, r, t] == ϕs[x, r, t] - ϕe[x, r, t] - U[SOCn[t]] + U[SOCp[t]]
       }}
```

Figure 5-1 : Snapshot of model developed in Mathematica environment

5.2.2 COMSOL 5.2

The model used for simulation was developed on COMSOL Multiphysics 5.2, adding on the work by Gregory Plett [25]. Conditional assumptions for the initial conditions were used in the model, using the capability of time delayed variables, to reach at agreeable results (something which the Mathematica didn't allow). There are a few equations that are not included in the model, especially the ones that cannot be differentiated with other results. Also, as the electrochemical model takes exponentially more time than the actual scale of time, it is not feasible to generate aging data for years and make a comparison. The work will compare the results against the general understanding of the degradation mechanism.

There are some equations omitted in the model to reduce the computation time, and the mystical limitations of the developed model. First, the ohmic heat generation has been estimated using the overall resistance of the cell, rather that the PDE representing the same. Further, the lithium plating behavior during the overcharge has not been incorporated in the model, because of inherent limitation of the model to go beyond the boundary conditions of electrode concentrations.

The nominal capacity of the modeled cell is 3.3 Ah, as discussed about in the last chapter, and for the testing variables it would be subjected to tests of various discharge rates of 0.5C to 10C.

Computation power and time

The workstation used for generating the results is the Dell Precision T1700: core i7 @3,4Ghz, with a RAM of 16GBs. With a time-step of 0.1 seconds, the time taken by the pseudo 3D model to simulate a 50 seconds of a modified hybrid power pulse characterization cycle is 37 seconds. Also, most processing of the data for calculating capacity loss has been done later.

The HPPC cycle has 2 second pulses of alternating charging and discharging with 1 second of rest, for 55 seconds, following 5 seconds of rest.

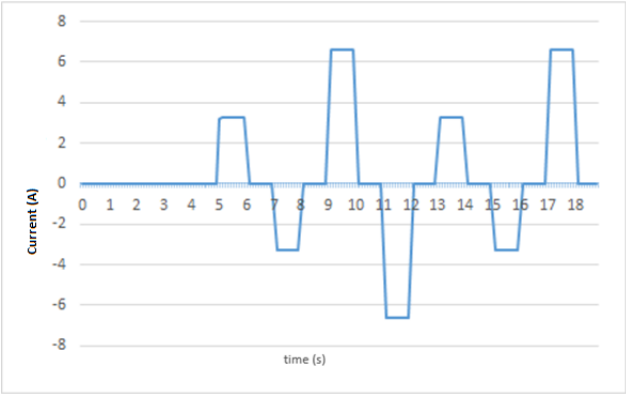

Figure 5-2 : Modified HPPC cycle with 1C and 2C discharge rates

5.3 Results

The first result that could be looked upon is the cell voltage profile. For an initial SOC of 0.65, the results are shown in Figure 5-2. It can clearly be seen that the initial estimate of the cell voltage was not correct for no current flow (like OCV). Such a set of partial differential equations could give a completely divergent set of results because of inconsistent initial conditions.

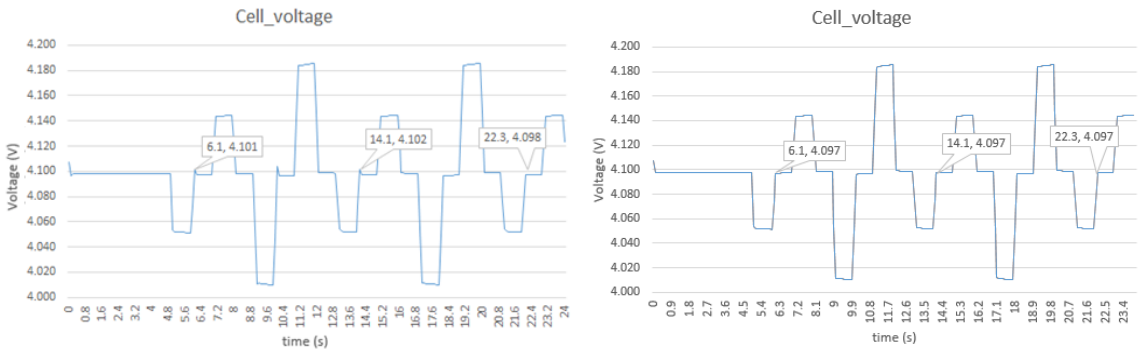

Figure 5-3: the cell voltage profile for the modified HPPC cycle with step a)0.1 b)0.01

However, this model is given a time of few seconds to stabilize the initial conditions. Further, with the same current discharge profile, the voltage overshoots are different (marginally). The overshoot is probably because of the charge transport, and it would be advisable to observe the electrolyte potential around the time stamps of the data callouts. There is not an apparent reason for why the electrolyte potentials should vary significantly for similar SOC and discharge current.

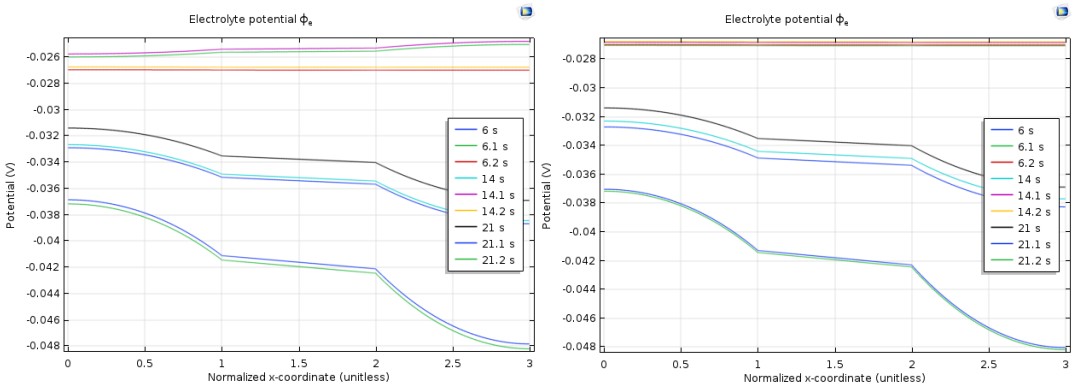

Figure 5-4 The electrolyte potential plots for the 3 callouts with step a) 0.1 s b)0.01 s

Again, if we see the results for a 0.01s step time, averaged over 0.1 seconds we see that the voltages values are more in agreement with each other. However, the electric potential of electrolyte still disagrees at the three steps, and the results from the two time-steps are very close to each other. Hence, selecting a right time-step could potentially generate varied results for such set of PDE's.

Seemingly a dichotomy, this thesis focuses on the aging mechanisms of Li-ion batteries, but it is very infeasible to generate aging data of years from an elaborate electrochemical model that runs on the same time-scale. It could be argued, however, that a full-scale model would rather help in developing a deeper understanding of battery design parameters and accelerate the development of batteries as it keeps getting closer to the real-life behavior of a battery. Hence, the results in this thesis try to inspect two aspects: first to inspect the model's behavior, and second to analyze the aging behavior with respect to the usage of the battery.

5.3.1 Peukert's law – rate of discharge

Peukert's law states that a battery tends to reflect different capacities at different charge rates of a battery. Even if this effect is much less pronounced in Lithium batteries as compared to a lead acid battery, this model could help us draw relations towards the aging behavior: Resistance increase and capacity degradation. Also, validity of this law could add a credibility to the model.

The current cycles which would be defined would ask for a same cumulative ampere-hour discharge from the battery, but at different rates. Starting from the same SOC, the plot

compares the end SOC's for different discharge rates. According to the plot 5-5, the Peukert's constant for the modeled battery came in the range of around 0.96~0.98, which seems accurate.

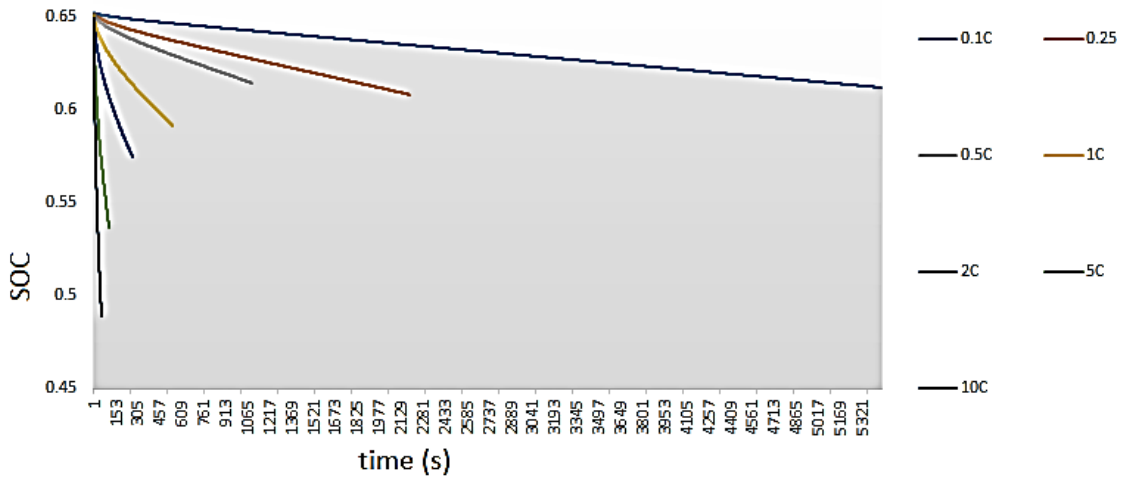

Figure 5-5 Peukert's law for a Li-ion battery

5.3.2 Capacity Degradation - SEI

The capacity degradation behavior does not depend completely on the high current, as can be deduced from Figure 5-6, in fact the 0.1C charge causes more SEI growth over a period of usage, as compared to the 10C discharge current. The growth of the SEI is homogenous throughout the electrodes.

It seems like a fair estimate for capacity degradation based on just the SEI density. Notice that the SEI density in the equations depends on the coefficient of the side reaction, and hence needs to be empirically correct.

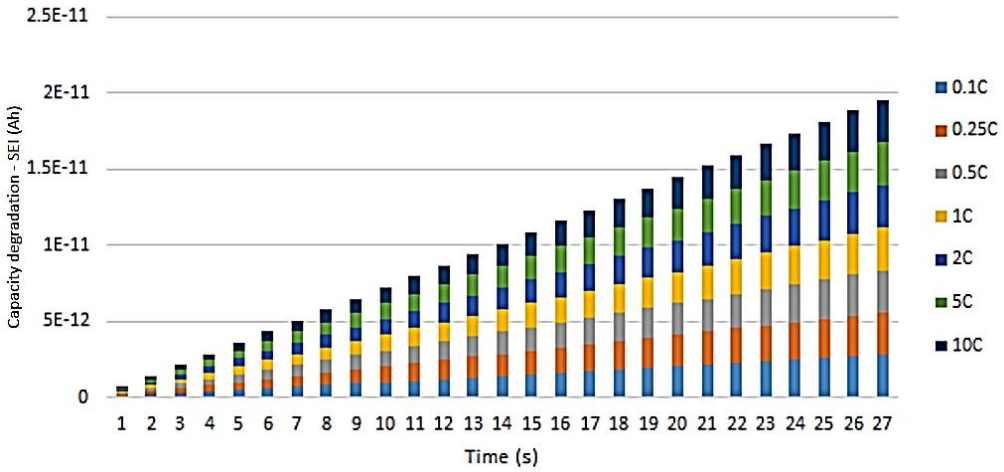

Figure 5-6 Capacity degradation for different current profiles

5.4 Conclusions

The developed model in the COMSOL environment does not capture all the capabilities of the suggested model. The limitations of existing software coupled with the available computational power for long simulations restricts the development of a full order model. These omissions of certain behaviors could be very sensitive to the dynamic behaviors of the battery. The heat equations will add significant amount of computational expense with the differential equations, even in only one spatial dimension of x.

However, the model developed generates similar behaviors as a real battery, evading the surprise as it is based on the existing porous electrode theory. The developed framework could now be used to target model order reduction techniques for capturing aging dynamics of a LIB. Further, a sensitivity analysis of the various parameters over the aging mechanisms could be done to develop a deeper design insight of the battery. This model could also be expanded with more varying parameters of diffusivity and conductivity with the length spatial dimension of the battery.

The use of python packages like DAE tools has not been explored in the thesis. There are open source applications like MPET [30], which can be used to simulate the developed model with modifications.

6 Summary and future work

This thesis introduces the modeling approaches of Lithium ion batteries, to finally draw the importance of physics-based models. As the model keep incorporating more and more physical processes, the easier it would become to shorten the design life of new batteries.

The existing approaches of continuum modeling and reduced order models are presented to make a qualitative comparison on how the prediction deviates with the assumptions made for reducing the model. The computational complexity of the produced model varies logarithmically, and the results further endorse the importance of the full order physics-based models. The parameters used in the model are discussed at length, explaining their physical significance and their scope. The methodologies of recording these variables empirically have been explored briefly, and ballpark values provide a reference to a battery designer.

The major contribution of the thesis is to bring various physical degradations of Lithium-ion batteries on a single interconnected set of partial differential equations. Even if the approach to the integration is simplistic, the integrated model tends to cover a lot of standardized aging mechanisms under the same roof of porous electrode theory model. There is a limitation of the model to be directly compared with aging results in the literature because of a large computational time, but the framework of this model can enable an engineer model most of the degradation processes of a LIB.

The thesis stands short of validating the development model in a simulation environment, and the ongoing work is towards using MPET open source package by DAE tools in python.

6.1 Uncertainties in an integrated model approach

As discussed before, PDE's are very complex to solve. For a minuscule change in the initial and boundary conditions, there can be paradigm shifts in the estimated solution of the equation. With every new variable added to the system, it simultaneously adds a degree of freedom and a need for boundary conditions to constraint it, hence, rapidly increasing the complexity. Any unspecified boundary gives results that are not unique, and don't define the actual behavior of the system.

With an increases number of PDE's and the suggested used of length varying variables, this model proposes an increase in uncertainly if the conditions are not properly defined. This increase in uncertainty questions the approach to bring all mechanisms together in an integrated theory. This topic is also debated in other fields of science like nuclear reactor modeling, and only a validated model could present an answer to the question.

6.2 Future work

The work achieved in this thesis would need complements in various domains, as the battery industry is evolving every day. Solid state batteries, sodium ions, and fuel cell-based chemistries might need foundational modifications in the model. Further, even if a model

framework integrating known mechanisms has been developed, there are degradation mechanisms that haven't been quantified with equations.

Firstly, the limitations in the original theory, as mentioned in the Chapter 3, need to be addressed for a successful implementation of this framework. Smith and Bazant [30] introduced a multiphase porous electrode theory to simulate the heterogeneity of the battery materials, and integrating this framework with their model could find applications in new battery materials including the solid phase electrolytes.

Secondly, there needs to be a better way to reduce these equations without losing the predictive quality. This section explores a method using neural networks to achieve the same and discusses work by fellow researchers to extend this model for solid state batteries, and automotive BMS applications.

6.2.1 Neural networks for reducing the sets of equation

This work was done during the summer 2018 Convention with Wolfram Research, the parent company making the Mathematica software. As the real-time solution of such a set of partial differential equations is not feasible for the mobile application of automotive applications, the idea behind this project was to find out if the finite element results could be used to train neural networks, and if they were a suitable choice to make faster predictions for these set of equations.

There has been work before using neural networks to make these predictions [72] [73], but however the approach taken in the papers is in aid with mathematical methods of reduction. Neural networks are used for the estimation of the coefficients of the reduced equations. In contrast, this work uses convolution layers to learn the results in form of images.

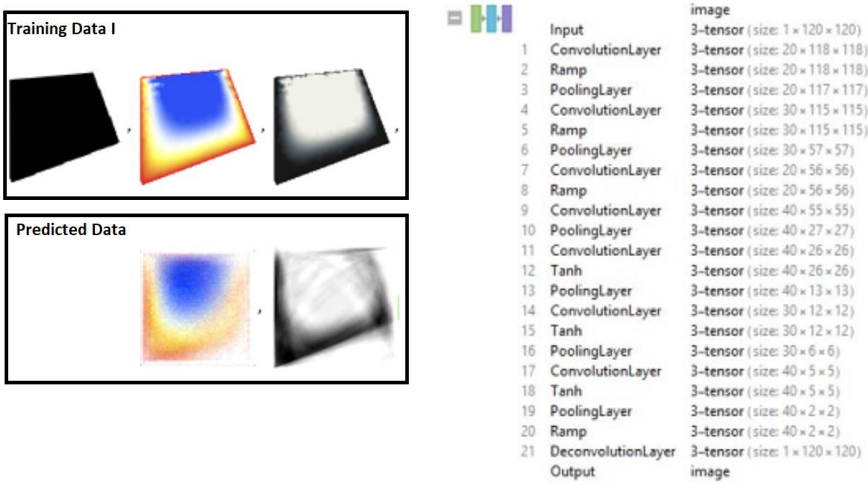

Figure 6-1 Training and predicted data, and snapshot of the Neural network

The first equation used is in the form shown in the following equation. This equation was solved for multiple thousands of shapes solved over a region made of 4 vertices, and this data was used to train a network made of 21 layers deep network, as shown in Figure 6-1.

$$\frac{\partial \varphi(x,y)}{\partial y} = a\frac{\partial^2 \varphi(x,y)}{\partial x^2} - b \qquad \text{Equation 50}$$

The Figure shows the subset of the test set, actual results, and the prediction results. The average accuracy achieved for the model was more than 95%, but the distribution of the error rates varied to around 10% of times. The error calculation was made by calculating the rms error of each pixel.

Further, this method was extended to the Fick's law of diffusion, i.e. a parabolic PDE varying with time. However, as the time domain comes into play, the two dimensions were reduced to just the x dimension, so that the images could be generated for training the network. Using a 2D array would be theoretically be the same for the neural network, but it would have been difficult to visualize the results.

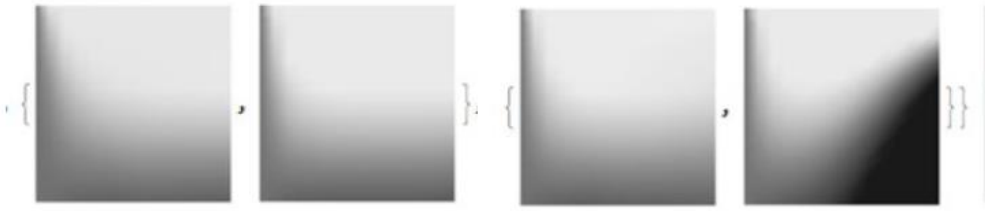

Figure 6-2 Data with 99% accuracy and 70% accuracy, concentration as a function of time

The generated results can be seen in the Figure 6-2, where two generated datasets are compared, with 99% accuracy of prediction, and with 70% accuracy. Here the non-linearity of the PDE makes it difficult for the neural network to make a good prediction. However, with increasing training time and the training data set, it was observed that the accuracy started improving to reach 95% of RMS image error. This validation proves that with increase in the training time, and the layers, neural networks as the universal function estimators could be a good contender of solving sets of PDEs.

The use targeted towards the model of batteries, would not use images but different battery parameters, and the usage data like current and temperature to predict the output variables like SOC and the degradation data. It can be argued that with a change in different coefficients of the PDE's the results could be highly non-linear, but a targeted training set for a specific Li-ion chemistry could constrain the variation set and it might be feasible for a neural network to heuristically predict the results.

The advantage of this method over the conventional testing data is that the PDE model could be used to generate data for conditions without using an actual workbench, and with increase in computational power it would shorten the time and expenses required to collect the data from a cell. This reduction could further enable extending the physical model to pack applications inexpensively.

Reference List

[1] X. Ding, X. Huang, J. Jin, H. Ming, L. Wang, and J. Ming, "Advanced and safer lithium-ion battery based on sustainable electrodes," *J. Power Sources*, vol. 379, no. January, pp. 53–59, 2018.

[2] S. S. Zhang, "A review on the separators of liquid electrolyte Li-ion batteries," *J. Power Sources*, vol. 164, no. 1, pp. 351–364, 2007.

[3] A. Subramania, N. T. Kalyana Sundaram, A. R. Sathiya Priya, and G. Vijaya Kumar, "Preparation of a novel composite micro-porous polymer electrolyte membrane for high performance Li-ion battery," *J. Memb. Sci.*, vol. 294, no. 1–2, pp. 8–15, 2007.

[4] V. A. Sethuraman, V. Srinivasan, A. F. Bower, and P. R. Guduru, "In Situ Measurements of Stress-Potential Coupling in Lithiated Silicon," *J. Electrochem. Soc.*, vol. 157, no. 11, p. A1253, 2010.

[5] J. L. Goldman, B. R. Long, A. A. Gewirth, and R. G. Nuzzo, "Strain anisotropies and self-limiting capacities in single-crystalline 3D silicon microstructures: Models for high energy density lithium-ion battery anodes," *Adv. Funct. Mater.*, vol. 21, no. 13, pp. 2412–2422, 2011.

[6] L. Lu, X. Han, J. Li, J. Hua, and M. Ouyang, "A review on the key issues for lithium-ion battery management in electric vehicles," *J. Power Sources*, vol. 226, pp. 272–288, 2013.

[7] R. Narayanrao, M. M. Joglekar, and S. Inguva, "A Phenomenological Degradation Model for Cyclic Aging of Lithium Ion Cell Materials," *J. Electrochem. Soc.*, vol. 160, no. 1, pp. A125–A137, 2012.

[8] M. Chen, S. Member, and G. a Rinc, "Accurate Electrical Battery Model Capable of Predicting Runtime and I – V Performance," vol. 21, no. 2, pp. 504–511, 2006.

[9] J. Wu, V. Srinivasan, J. Xu, and C. Y. Wang, "Newton-Krylov-Multigrid Algorithms for Battery Simulation," *J. Electrochem. Soc.*, vol. 149, no. 10, p. A1342, 2002.

[10] K. Smith, E. Wood, S. Santhanagopalan, G.-H. Kim, Y. Shi, and A. Pesaran, "Predictive Models of Li-ion Battery Lifetime," *IEEE Conf. Reliab. Sci. Adv. Mater. Devices*, p. 30, 2014.

[11] K. Uddin, A. Picarelli, C. Lyness, N. Taylor, and J. Marco, "An acausal Li-ion battery pack model for automotive applications," *Energies*, vol. 7, no. 9, pp. 5675–5700, 2014.

[12] D. Shin, M. Poncino, E. Macii, and N. Chang, "A statistical model of cell-to-cell variation in Li-ion batteries for system-level design," *Proc. Int. Symp. Low Power Electron. Des.*, no. i, pp. 94–99, 2013.

[13] C. Edouard, M. Petit, C. Forgez, J. Bernard, and R. Revel, "Parameter sensitivity analysis of a simplified electrochemical and thermal model for Li-ion batteries aging," *J. Power*

Sources, vol. 325, pp. 482–494, 2016.

[14] R. E. Gerver, "3D Thermal-Electrochemical Lithium-Ion Battery Computational Modeling," *Engineering*, 2009.

[15] D. Li, D. Danilov, Z. Zhang, H. Chen, Y. Yang, and P. H. L. Notten, "Modeling the SEI-Formation on Graphite Electrodes in LiFePO4 Batteries," *J. Electrochem. Soc.*, vol. 162, no. 6, pp. A858–A869, 2015.

[16] K. An, P. Barai, K. Smith, and P. P. Mukherjee, "Probing the Thermal Implications in Mechanical Degradation of Lithium-Ion Battery Electrodes," *J. Electrochem. Soc.*, vol. 161, no. 6, pp. A1058–A1070, 2014.

[17] R. D. Perkins, A. V. Randall, X. Zhang, and G. L. Plett, "Controls oriented reduced order modeling of lithium deposition on overcharge," *J. Power Sources*, vol. 209, pp. 318–325, 2012.

[18] A. Allam and S. Onori, "Characterization of aging propagation in Lithium-ion cells based on an electrochemical model," *Proc. Am. Control Conf.*, vol. 2016–July, pp. 3113–3118, 2016.

[19] J. W. T. Newman, "Porous - electrode theory with battery applications," pp. 1–2, 1975.

[20] V. Viswanathan, "Fundamental Challenges Facing Next-Generation Li Ion Batteries," *J. Phys. Chem. Lett.*, vol. 6, no. 22, pp. 4673–4674, 2015.

[21] R. P. Muller and P. A. Schultz, "Modelling challenges for battery materials and electrical energy storage," *Model. Simul. Mater. Sci. Eng.*, vol. 21, no. 7, 2013.

[22] A. Falconi, "Electrochemical Li-Ion battery modeling for electric vehicles To cite this version : HAL Id : tel-01676976 Modélisation électrochimique du comportement d ' une cellule Li-ion pour application au véhicule électrique," 2018.

[23] A. Millner, "Modeling lithium ion battery degradation in electric vehicles," *2010 IEEE Conf. Innov. Technol. an Effic. Reliab. Electr. Supply, CITRES 2010*, no. October 2010, pp. 349–356, 2010.

[24] E. Prada, D. Di Domenico, Y. Creff, J. Bernard, V. Sauvant-Moynot, and F. Huet, "A Simplified Electrochemical and Thermal Aging Model of LiFePO4-Graphite Li-ion Batteries: Power and Capacity Fade Simulations," *J. Electrochem. Soc.*, vol. 160, no. 4, pp. A616–A628, 2013.

[25] Gregory L. Plett, *Battery Management Systems, Volume 1*, vol. I. 2015.

[26] C. Zou, C. Manzie, and D. Nesic, "A Framework for Simplification of PDE-Based Lithium-Ion Battery Models," *IEEE Trans. Control Syst. Technol.*, vol. 24, no. 5, pp. 1594–1609, 2016.

[27] M. Doyle, T. F. Fuller, and J. Newman, "Modeling of Galvanostatic Charge and Discharge of the Lithium / Polymer / Insertion Cell," vol. 140, no. 6, pp. 1526–1533, 1993.

[28] Y. Lai *et al.*, "Insight into heat generation of lithium ion batteries based on the electrochemical-thermal model at high discharge rates," *Int. J. Hydrogen Energy*, vol. 40, no. 38, pp. 13039–13049, 2015.

[29] P. W. C. Northrop, M. Pathak, D. Rife, S. De, S. Santhanagopalan, and V. R. Subramanian, "Efficient Simulation and Model Reformulation of Two-Dimensional Electrochemical Thermal Behavior of Lithium-Ion Batteries," *J. Electrochem. Soc.*, vol. 162, no. 6, pp. A940–A951, 2015.

[30] R. B. Smith and M. Z. Bazant, "Multiphase Porous Electrode Theory," vol. 164, no. 11, 2017.

[31] T. Jacobsen and K. West, "Diffusion impedance in planar, cylindrical and spherical symmetry," vol. 40, no. 94, 1995.

[32] V. R. Subramanian, V. D. Diwakar, and D. Tapriyal, "Efficient Macro-Micro Scale Coupled Modeling of Batteries," *J. Electrochem. Soc.*, vol. 152, no. 10, p. A2002, 2005.

[33] V. Ramadesigan, V. Boovaragavan, J. C. Pirkle, and V. R. Subramanian, "Efficient Reformulation of Solid-Phase Diffusion in Physics-Based Lithium-Ion Battery Models," *J. Electrochem. Soc.*, vol. 157, no. 7, p. A854, 2010.

[34] M. Safari, M. Morcrette, A. Teyssot, and C. Delacourt, "Multimodal Physics-Based Aging Model for Life Prediction of Li-Ion Batteries," *J. Electrochem. Soc.*, vol. 156, no. 3, p. A145, 2009.

[35] Y. Dai, L. Cai, and R. E. White, "Capacity Fade Model for Spinel LiMn2O4 Electrode," *J. Electrochem. Soc.*, vol. 160, no. 1, pp. A182–A190, 2013.

[36] C. Delacourt and M. Safari, *Mathematical Modeling of Aging of Li-Ion Batteries*. 2016.

[37] K. Smith, Y. Shi, and S. Santhanagopalan, "Degradation mechanisms and lifetime prediction for lithium-ion batteries — A control perspective," *2015 Am. Control Conf.*, pp. 728–730, 2015.

[38] P. Barai, K. Smith, C.-F. Chen, G.-H. Kim, and P. P. Mukherjee, "Reduced Order Modeling of Mechanical Degradation Induced Performance Decay in Lithium-Ion Battery Porous Electrodes," *J. Electrochem. Soc.*, vol. 162, no. 9, pp. A1751–A1771, 2015.

[39] G. Wertheim, "Electronic structure of lithium graphite," *Solid State Commun.*, vol. 33, no. 11, pp. 1127–1130, 1980.

[40] R. Xu and K. Zhao, "Electrochemomechanics of Electrodes in Li-Ion Batteries: A Review," *J. Electrochem. Energy Convers. Storage*, vol. 13, no. 3, p. 030803, 2016.

[41] M. J. Brand *et al.*, "Effects of vibrations and shocks in electric vehicles on Li-ion batteries," *EVS28 Int. Electr. Veh. Symp. Exhib.*, vol. 288, pp. 1–17, 2015.

[42] J. M. Hooper, J. Marco, G. H. Chouchelamane, J. S. Chevalier, and D. Williams, "Multi-axis vibration durability testing of lithium ion 18650 NCA cylindrical cells," *J. Energy Storage*, vol. 15, pp. 103–123, 2018.

[43] R. Fu *et al.*, "Vibration-induced changes in the contact resistance of high power electrical connectors for hybrid vehicles," *IEEE Trans. Components, Packag. Manuf. Technol.*, vol. 2, no. 2, pp. 185–193, 2012.

[44] L. Somerville *et al.*, "Impact of vibration on the surface film of lithium-ion cells," *Energies*, vol. 10, no. 6, pp. 0–12, 2017.

[45] C. R. Pals, "Thermal Modeling of the Lithium/Polymer Battery," *J. Electrochem. Soc.*, vol. 142, no. 10, p. 3282, 1995.

[46] Y. Yue and H. Liang, "3D Current Collectors for Lithium-Ion Batteries : A Topical Review," vol. 1800056, pp. 1–20, 2018.

[47] J. Catton, "Calendar Aging and Lifetimes of LiFePO4 Batteries and Considerations for Repurposing," 2017.

[48] D. Li, *Aging mechanisms of Li-ion batteries : seen from an experimental and simulation point of view*. 2017.

[49] P. W. C. Northrop, V. Ramadesigan, S. De, and V. R. Subramanian, "Coordinate Transformation, Orthogonal Collocation, Model Reformulation and Simulation of Electrochemical-Thermal Behavior of Lithium-Ion Battery Stacks," *J. Electrochem. Soc.*, vol. 158, no. 12, p. A1461, 2011.

[50] V. Ramadesigan, P. W. C. Northrop, S. De, S. Santhanagopalan, R. D. Braatz, and V. R. Subramanian, "Modeling and Simulation of Lithium-Ion Batteries from a Systems Engineering Perspective," *J. Electrochem. Soc.*, vol. 159, no. 3, pp. R31–R45, 2012.

[51] G.-H. Kim, K. Smith, K.-J. Lee, S. Santhanagopalan, and A. Pesaran, "Multi-Domain Modeling of Lithium-Ion Batteries Encompassing Multi-Physics in Varied Length Scales," *J. Electrochem. Soc.*, vol. 158, no. 8, p. A955, 2011.

[52] S. Santhanagopalan, Q. Guo, and R. E. White, "Parameter Estimation and Model Discrimination for a Lithium-Ion Cell," *J. Electrochem. Soc.*, vol. 154, no. 3, p. A198, 2007.

[53] Y. Zeng, "Mathematical Modeling of Lithium-ion Intercalation Particles and Their Electrochemical Dynamics," no. 2011, 2011.

[54] H. Arunachalam, S. Onori, and I. Battiato, "On Veracity of Macroscopic Lithium-Ion Battery Models," *J. Electrochem. Soc.*, vol. 162, no. 10, pp. A1940–A1951, 2015.

[55] E. Hosseinzadeh, J. Marco, and P. Jennings, "Optimisation of Lithium-Ion Battery Design Parameters Using Analysis of Variance," 2017.

[56] C. Lin and A. Tang, "Simplification and efficient simulation of electrochemical model for Li-ion battery in EVs," *Energy Procedia*, vol. 104, pp. 68–73, 2016.

[57] J. Li *et al.*, "3D simulation on the internal distributed properties of lithium-ion battery with planar tabbed con fi guration," *J. Power Sources*, vol. 293, pp. 993–1005, 2015.

[58] J. Cho, "Measured Mass Transfer Coefficients in Porous Media Using Specific Interfacial Area," pp. 7883–7888, 2005.

[59] E. Billy, M. Joulie, R. Laucournet, A. Boulineau, E. De Vito, and D. Meyer, "Emmanuel Billy, * , † , ǂ Marion Joulie ,́ † , ǂ Richard Laucournet, † , ǂ Adrien Boulineau, † , ǂ Eric De Vito, † , ǂ and Daniel Meyer § † ǂ," pp. 2–13, 2018.

[60] G. B. Less *et al.*, "Micro-Scale Modeling of Li-Ion Batteries : Parameterization and Validation," vol. 159, no. 6, 2012.

[61] and V. R. Venkatasailanathan Ramadesigan, Vijayasekaran Boovaragavan and Subramanian, "Efficient Reformulation of Solid-Phase Diffusion in Physics-Based Lithium-Ion Battery Models," vol. 16, no. 29, pp. 129–134, 2009.

[62] A. Munar, A. Andrio, R. Iserte, and V. Compañ, "Ionic conductivity and diffusion coef fi cients of lithium salt polymer electrolytes measured with dielectric spectroscopy," *J. Non. Cryst. Solids*, vol. 357, no. 16–17, pp. 3064–3069, 2011.

[63] M. Klett, *Electrochemical Studies of Aging in Lithium-Ion Batteries*. .

[64] J. N. Reimers, "Transport Properties of LiPF 6 -Based Li-Ion Battery Electrolytes," pp. 882–891, 2005.

[65] M. Guo and R. E. White, "A distributed thermal model for a Li-ion electrode plate pair," *J. Power Sources*, vol. 221, pp. 334–344, 2013.

[66] A. Nyman, T. G. Zavalis, R. Elger, M. Behm, and G. Lindbergh, "Analysis of the Polarization in a Li-Ion Battery Cell by Numerical Simulations," pp. 1236–1246, 2010.

[67] S. Zugmann, M. Fleischmann, M. Amereller, R. M. Gschwind, H. D. Wiemhöfer, and H. J. Gores, "Electrochimica Acta Measurement of transference numbers for lithium ion electrolytes via four different methods , a comparative study," *Electrochim. Acta*, vol. 56, no. 11, pp. 3926–3933, 2011.

[68] L. B. Cell and S. Dey, "ESTIMATION OF LITHIUM-ION CONCENTRATIONS IN BOTH ELECTRODES OF A LITHIUM-ION BATTERY CELL," pp. 1–9, 2015.

[69] P. W. C. Northrop, B. Suthar, V. Ramadesigan, S. Santhanagopalan, R. D. Braatz, and V.

R. Subramanian, "Efficient Simulation and Reformulation of Lithium-Ion Battery Models for Enabling Electric Transportation," *J. Electrochem. Soc.*, vol. 161, no. 8, pp. E3149–E3157, 2014.

[70] G. Fan, K. Pan, and M. Canova, "A comparison of model order reduction techniques for electrochemical characterization of Lithium-ion batteries," *2015 54th IEEE Conf. Decis. Control*, vol. 2016–Febru, no. Cdc, pp. 3922–3931, 2015.

[71] J. Rivera-Barrera, N. Muñoz-Galeano, and H. Sarmiento-Maldonado, *SoC Estimation for Lithium-ion Batteries: Review and Future Challenges*, vol. 6, no. 4. 2017.

[72] L. Ruthotto and E. Haber, "Deep Neural Networks motivated by Partial Differential Equations," pp. 1–7, 2018.

[73] J. Tompson, K. Schlachter, P. Sprechmann, and K. Perlin, "Accelerating Eulerian Fluid Simulation With Convolutional Networks," 2016.